CHALMERS

Physical modeling of percussion instruments

Thesis for the degree of Master of Science in Physics Engineering

ANDERS GÄRDER

Department of Civil and Environmental Engineering
Division of Applied Acoustics
Room Acoustics Group
CHALMERS UNIVERSITY OF TECHNOLOGY
Göteborg, Sweden 2005

Master's Thesis 2005:23

Physical Modeling of Percussion Instruments

ANDERS GÄRDER

Department of Civil and Environmental Engineering
Division of Applied Acoustics
Room Acoustics Group
CHALMERS UNIVERSITY OF TECHNOLOGY
Göteborg, Sweden 2005

Cover:

Illustration, originally from Lewis Carrol's "Through the Looking-Glass", drawn by Sir John Tenniel in 1872.

Physical modeling of percussion instruments
Svensk titel: Fysikalisk modellering av slaginstrument
ANDERS GÄRDER
Department of Civil and Environmental Engineering
Division of Applied Acoustics
Room Acoustics Group
Chalmers University of Technology

Abstract

This report contains an overview of a typical modern rock drum set and the acoustics describing them. Explanations of the modeling methods Digital Waveguides and Digital Waveguide Networks are given and then applied to simulating a tom tom drum. The results are compared to recordings of real tom tom drums made in an anechoic environment. Although clearly distinguishable from real drum sounds, basic acoustic properties are accurately modeled and the model can be used as a basis for more detailed physical modeling.

Keywords:

Acknowledgements

I would like to thank the following people who have helped me with this thesis:

This document was written in LaTeX using the Lyx document processor, more information about this excellent program can be found at *www.lyx.org*.

Contents

1 Introduction

1.1 Background and scope of this thesis

This work was initiated by me as a project to find new exciting drum models for a drum machine being developed by the synthesizer company Elektron ESI AB. Our initial idea was to get hold of the best algorithms for generating the sounds of a rock drum set in real time in CD quality. However, the scope of project changed considerably to a more scientific line of creating a working model of a rock drum using physical modeling. As a lot of research has been focused on the method called 'Digital Waveguides' the last decade, this was the modeling method of choice.

1.2 The structure of this document

This paper will discuss the general concept of waveguides (section 3), their strengths and weaknesses. Techniques for getting rid of unwanted effects like dispersion and connecting several components together to create more complex structures will be presented. These methods will then be applied specifically to model a drum (section 4). Section 2 describes the basic components of a rock drum set and defines the terminology used in this document. It also contains a description of the mathematical equations governing the propagation of sound waves in materials and air including the assumptions and simplifications I have assumed.

The models have been implemented in MATLAB™, an interpreted language suitable for mathematical synthesis and analysis in general and especially matrix manipulations. The implementation with source code is available in Appendix B. A report on measuring parameters and recording sounds from real tom tom drums is presented in Appendix C.

1.3 A note on the state of the art of commercial drum modeling

Due to the computational complexity few commercial synthesizers offer physical modeling of drums. As of 2004 two machines have claimed to use this, the first was the Korg Wavedrum™ and the manufacturer Roland offers V-drums™ (which is rumored to be a sample player with sophisticated filters internally). Unfortunately, the exact implementations used in these machines are corporate secrets and, as is very common in the audio industry, the general area is heavily protected by patents.

Modeling of acoustic drums has apparently not been a major commercial success yet, and most of the synthesizer manufacturers today are instead concentrating on modeling old analog electronic drumboxes using traditional oscillator and filtering techniques. Also, as audio synthesis in recent years has successfully moved into the home computer, cheap computer memory has made immense multisampling of instruments (libraries several gigabytes large are common) possible, delivering realism and variety.

2 Drums and the physics behind them

2.1 The terminology of drums

First let us introduce the components of a drum and their functions.

- Battering head: This is the membrane struck by the drummer. It is the component that has to be replaced most often on a drum.

- Resonant head: This is an optional head on the bottom of the drum, usually it is thinner than the battering head. It is tuned to the battering head, either higher or lower.

- Rim: These components hold the drum heads in place. They are tightened using the tuning bolts to tune the drum. Some drummers also strike the rim to produce the sound labelled the rim shot.

- Shell: The body of the drum can be made of several different materials, the most usual being glassfiber or wood (for example maple). The wood is often layered in 5 to 10 plys. Glassfiber gives a harder sound than wood that tends to absorb more high frequencies.

- Tuning bolts: These are used to tighten the heads to give the desired pitch. Usually there are 6 or 8 bolts evenly distributed around the rim. To tune a drum it is essential to get an even tension of the membrane so that the drum sounds similar being hit on a common radius from the center.

Figure 2.1: The components of a drum.

Figure 2.2: A picture of a typical drum set.

2.2 The typical rock drum set

2.2.1 The different components of the drum set

The basic rock drum set is composed of the following percussion instruments:

- Bass drum: This large drum is played with a pedal attached to a felt hammer. The bass drum is usually between 18 and 26″ in diameter.

- Tom tom drums: A drum set often contains several tom toms of different sizes, from 8 to 18″, either mounted over the bass drum or standing on the floor.

- Snare drum:A typical snare is 13 or 14″ in diameter with a depth between 5 and 8″. The snare is less deep than a tom tom drum, but its main feature is snares (metal wires)fitted against the resonant head. The tightness between the head and the snares can be adjusted.

- Cymbals: There are a lot of different cymbals with varying purposes:

  - The ride cymbal, that is often played continuously in the rhythm, is usually 18,20 or 22″ in diameter. It has a more ringing sound than the crash cymbal.

  - The crash cymbal is mainly used in fills and has a typical diameter of 14,16 or 18″.

  - Effect cymbals; like a bell, china or gong are used to add character to the rhythm and vary greatly in sound and size.

- Hi-hats: A hi-hat is two cymbals placed opposite to each other on an axis. It can be opened or closed using a pedal and is played in this way or in combination with drumsticks. A hi-hat cymbal is 13,14 or 15″ in diameter.

4

2.2.2 The shell of the drum

The shell is made from amongst others wood, glass fiber or plexi glass. Wood is an orthotropic material with properties varying even on the same tree. However drum shells are generally made out of several plys which gives more isotropic behavior. The parameters of Plexi Glass are taken from the Mat Web Online Materials Information Resource and are not guaranteed to be directly applicable to any brand or type of drum in use. The Poissons ratio of an orthotropic material is described by a tensor but as a first approximation of modeling stiffness waves in the shell the ratio can probably be taken as a constant. This is because the different plys of wood are oriented normally to each other to give the material even properties in all directions.

Table 2.1: Properties of plexi glass

Physical property	Value
Density	1190 kg/m^3
Modulus of elasticity	3.3 GPa
Poissons ratio	0.37

Table 2.2: Properties of wood (taken from [4])

Physical property	Value
Density	500 kg/m^3
Modulus of elasticity (longitudinal)	5-16 GPa
(radial)	0.7-2.2 GPa
(Tangentional)	0.4-1.1 GPa
Poissons ratio	0.25-0.5

2.2.3 Drum heads

Drum heads for rock drums are made of mylar (polyethylene terephtalate). Drum heads for concert drums are sometimes of animal skin like calfskin but this is becoming a rare luxury. Mylar drum heads come in several different variations

- Single layer heads, these are generally 'clear' or 'smooth white' where the white heads have a rugged surface suitable for playing with brushes.

- Double layer heads separated by a layer of thin oil, these have a less bright sound than single layer heads.

- Resonant heads are generally thinner and less durable as they are not supposed to be hit.
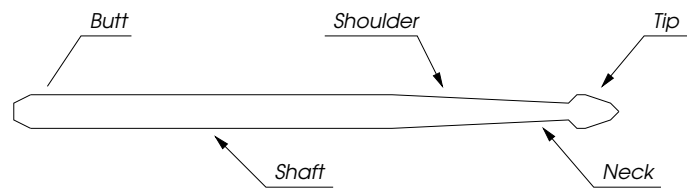
Figure 2.3: The different parts of a drum stick

The battering heads are generally between 0.25 and 0.5 mm thick with a density between 0.2 and $0.5\,kg/m^2$. Mylar has a modulus of elasticity of $E = 3.5\,GPa$.

2.2.4 Drum sticks

Drums can, of course, be played in a number of ways, including with the bare hands, but the most common way is to use drum sticks. In rock or jazz playing these are made of wood, in an orchestral setting a felt hammer is often used. A typical wood stick is 40 cm in length, weighs between 40 and 80 grams and is made of American hickory or maple.

- Heavy sticks are considered to give a richer spectrum of frequencies than light sticks.

- Hard wood gives a richer spectrum than soft wood.

- A small tip generates more high frequency components than a larger one.

- The shape of the tip gives the player an opportunity to vary the area of contact, these are some typical shapes:

  - Cone shape: Gives a small area of contact and a clear, light sound.

  - Round shape: Gives a darker sound that is hard to vary, the tip always hits the skin in the same manner.

  - Oval shape: Depending on the angle of impact this can be varied between the darker sound of the round shape and the lighter of the cone shape.

2.3 Equations governing sound propagation

2.3.1 Propagation in air

The equation of a wave propagating in gas is
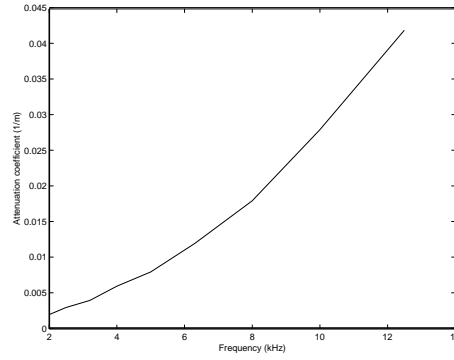
Figure 2.4: Attenuation factor of sound waves in air at 50% relative humidity taken from [5].

$$\frac{\partial^2 p}{\partial t^2} = \frac{B}{\rho} \nabla^2 p$$

where p is the sound pressure, B is the bulk modulus and ρ is the density of the gas. Sound propagation in free air is, except for very high frequencies, an adiabatic process and therefore, as a consequence of thermodynamics, $B = \gamma p_0$ where $\gamma = \frac{C_p}{C_v} = 1.4$ and p_0 is the average air pressure, so $B = 1.42$ kPa. This gives the speed of propagation $c = \sqrt{\frac{\gamma p_o}{\rho}}$. The speed can also be calculated from the temperature T (Celsius) and the approximate relationship is $c \approx 332(1 + 0.00166T)\,m/s$ which gives $c = 346\,m/s$ at 25°C.

For the free plane wave the relation between the pressure, p, and the velocity of compression, u, can be written as $p = Zu$, where $Z = \rho c$ is called the wave impedance. For air $\rho \approx 1.19\,kg/m^3$ giving an impedance of $410 kgm^{-2}s^{-1}$.

The boundary condition for of a plane pressure wave at a rigid wall is

$$\hat{n} \cdot \nabla p = 0 \tag{2.1}$$

where $\hat{n}$ is normal to the boundary. Also, an equivalent boundary condition is $\hat{n} \cdot u = 0$.

Sound waves traveling through air suffers frequency dependent attenuation as seen in figure 2.4. There are also many non linear phenomena present in air that are not dealt with here or included in the model.

2.3.2 Propagation in membranes, plates and shells

The wave equation in an ideal membrane can be written

$$\frac{\partial^2 z}{\partial t^2} = \frac{K}{\sigma} \left(\frac{\partial^2 z}{\partial x^2} + \frac{\partial^2 z}{\partial y^2} \right) \tag{2.2}$$

7
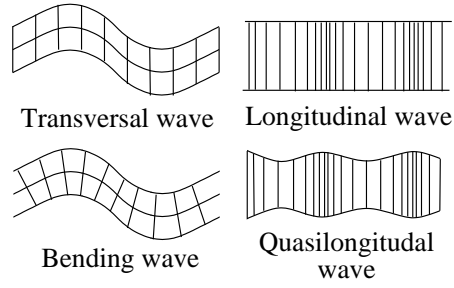
Figure 2.5: The different kinds of waves propagating in a plate.

where K is the tension and σ is the area density of the membrane.

An important difference between the ideal membrane and plates or shells (and non-ideal membranes) is the presence of stiffness and the ability to withstand compression.This gives rise to effects such as longitudinal waves and bending waves as opposed to the transversal waves of the ideal membrane. In fact true longitudinal waves are not possible in a plate of limited size, instead quasi-longitudinal waves occur. The different wave types are illustrated in figure 2.5. Bending waves are the waves that couple to air the best.

The speed of propagation of a longitudinal wave is $c_l = \sqrt{\frac{E}{\rho(1-\nu^2)}}$ where E is Young's modulus, ρ is the density and ν is the Poisson ratio. A quasi-longitudinal wave travels at the speed $c_{ql} = \sqrt{\frac{E(1-\nu)}{\rho(1+\nu)(1-2\nu)}}$. Transversal waves in plates propagate with $c_T = \sqrt{\frac{G}{\rho}}$, where G is the shear modulus, indicating that mainly shear stresses are involved.

Equation 2.3 describes a membrane with transversal waves and stiffness giving rise to bending waves

$$\frac{\partial^2 z}{\partial t^2} = \frac{K}{\sigma}\nabla^2 z - \frac{h^2 E}{12\rho(1-v^2)}\nabla^4 z \tag{2.3}$$

If a wave, $y = Ae^{j(kx-\omega t)}$, where ω is the angular frequency, is moving freely on the membrane and we define the stiffness $S^4 = \frac{h^2 E}{12\rho(1-v^2)}$ equation 2.3 can be written as

$$\frac{\partial^2 y}{\partial t^2} = -\left(c^2 + \frac{k^2 S^4}{\epsilon}\right)k^2 y$$

Comparing this equation to the equation of the ideal membrane $\frac{\partial^2 y}{\partial t^2} = -c^2 k^2 y$ and assuming that $k = \frac{\omega}{c}$ we get the following expression for the speed of propagation

$$c(\omega) = c_0\sqrt{1 + \frac{S^4\omega^2}{\sigma c_0^4}} \tag{2.4}$$

which may serve as an approximation of the effects of bending waves in a shell or membrane.

3   The theory of waveguides

3.1   History of the waveguides

The first attempts to use the approach of wave guides for solving physical problems were done in the early seventies, it has since been in use in the field of Electromagnetic wave calculations known as the Transmission-Line Modeling Method [1]. In 1983 Karplus and Strong presented the Karplus-Strong algorithm [2]. This was an ad hoc technique involving a delay line that could successfully model the sound of a vibrating string. The same year Julius Smith and David Jaffe connected the method to physical theory and Julius Smith developed the concept into what has become known as digital waveguides [3]. The method proved to be a powerful method for simulating the behavior of musical instruments whose sound generation is one dimensional, in fact it provided a correct solution of the band limited wave equation. The success of the method led to implementation in a series of Yamaha synthesizers under the name 'Physical Modeling', which provided brass, reed and string instruments. Lack of processing power however led to limited polyphony and low commercial success. In 1993 the concept was expanded to 2 dimensional waveguides and then N dimensional waveguides with Julius Smith still leading the way [6]. In recent years Lauri Savioja and Vesa Välimäki et al at Helsinki University of Technology, among others, have been successful in developing these algorithms further [9][10].

3.2   The one dimensional waveguide

A one dimensional waveguide is simply a simulation of the bandlimited solution of the wave equation (3.1):

$$\frac{1}{c^2}\frac{\partial^2 y}{\partial t^2} = \frac{\partial^2 y}{\partial x^2} \tag{3.1}$$

In an ideal string $c = \sqrt{\frac{K}{\epsilon}}$ where K is the string string tension (N) and ϵ is the linear mass density (kg/m). The general solution to this problem without imposing any boundary conditions, like clamping, is the sum of two arbitrary functions moving left and right at the speed c (equation (3.2)).

$$y(t,x) = y_{right}(x - ct) + y_{left}(x + ct) \tag{3.2}$$

In figure 3.1 the upper figure shows two functions traveling in different directions on an elastic string clamped at both ends. The figure below it gives a symbolic view of
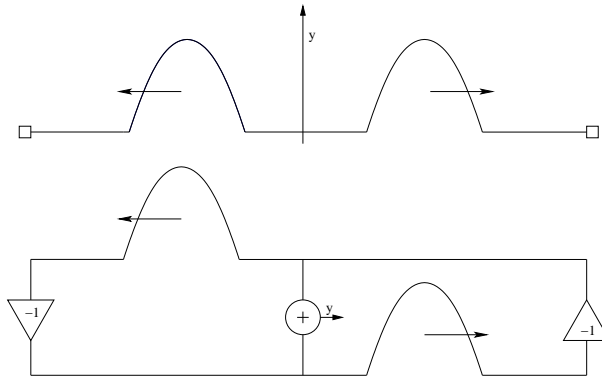
Figure 3.1: The solution of the one dimensional wave equation. (Above) A wave moving on an ideal string with clamped ends (Below) The principle behind a wave guide simulating the string.

what is happening and also gives a good clue on how a one dimensional wave guide is implemented. By discretising the string into N steps the waves can be represented by two vectors, one representing the wave moving left and one the wave moving right (the two wave guides). The elements are then shifted in their respective directions and the two elements at the clamping are treated to the boundary conditions (in the case of clamping; inversion) and then the element is inserted into the vector being shifted the other way (the wave has been reflected). Extracting the signal at any point is done by adding the elements of the two vectors at that point. The length of the string l, the speed of propagation c, the number of elements N in the waveguides and the temporal sample frequency of the sound F_s are related as follows:

$$N = \frac{F_s \cdot l}{c}$$

As N is an integer every length l is not obtainable unless a fractional delay is introduced somewhere, typically at the ends of the waveguides [11].

Damping can be done by filtering the waves in each point they pass or simply lumping the damping together and doing it at critical points (where the values have to be used in further calculations). For example can frequency independent damping be converted from multiplying every element with d to assuming that the element has moved N steps since it was last damped and multiplying it with d^N. This approach works as long as transformations are linear.

One problem remaining is introducing the traveling waves into the waveguides. This can be done by introducing an initial wave at $t = 0$ in the waveguides and then starting the process. The real power, though, comes from being able to introduce new excitations during the simulation. Being able to create physically correct or sonically convincing excitations is of great importance as the first transient part of a sound is what the brain uses to identify the sound. The challenge is to simulate the behavior of the exciter and its interaction with the string. The most useful wave variable isn't displacement, but velocity, having the advantage of being easily transformed into force waves

by the transformation

$$f_{left}(n) = -Zv_{left}(n)$$
$$f_{right}(n) = Zv_{right}(n)$$

where $Z = \sqrt{K\epsilon}$ is the wave impedance for the ideal string and the positive direction of the force $f = f_{left} + f_{right}$ is upwards. As these relations are central in modeling reflections when waves move thru material with changing properties, the derivation of these equations is available in Appendix A.

Sometimes the strings need to be connected and interacting. For example strings on a guitar interact mainly by vibrations moving between them thru the bridge of the guitar. This is modeled by introducing the lossless scattering junction, this is also the basis of N-dimensional wave guide modeling and is therefore introduced in section 3.3.

3.3   An N-dimensional waveguide mesh

The wave equation of arbitrary dimensions can be written as

$$\frac{1}{c^2}\frac{\partial^2 f}{\partial t^2} = \sum_{i=1}^{N}\frac{\partial^2 f}{x_i^2} \tag{3.3}$$

where N is the dimension. The following discussion will mainly deal with implementing simulations of the two and three dimensional wave equation as these are relevant to real world physics. Sounds created from four dimensional simulations are however an interesting and thrilling concept.

3.3.1   The lossless scattering junction

To connect waveguides together the concept of the lossless scattering junction was introduced. The scattering junction can be seen as the bridge of a guitar where the strings interact or the junction of some acoustic tubes. Julius Smith proposed that these junctions could be used to extend the concept of waveguides to N dimensions. The theory assumes that a wave impedance R can be defined. In this section strings will be used to design a membrane so $f = Zv$ where v is the transverse velocity. The following assumptions are made about the junction.

- N Waveguide pairs are connected to the junction

- As the waveguides are physically connected at the junction all the incoming waveguides must have the same value v_j in that point.

11
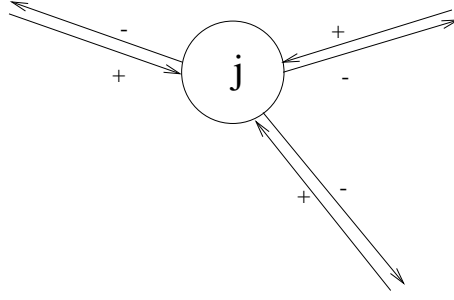
Figure 3.2: Three waveguide pairs connected to a junction.

- The junction is weightless and therefore all forces must cancel there or the junction would accelerate infinitely.

This is summarized in equation 3.4, with N waveguide pairs

$$\begin{cases} \sum_{i=1}^{N} f_i = 0 \\ v_i = v_j \end{cases} \tag{3.4}$$

The transversal velocity v is always the sum of the waves moving in the incoming and outgoing waveguide even at the junction so $v_j = v_{i-} + v_{i+}$, where v_{i+} is the incoming and v_{i-} is the outgoing waveguide of the ith waveguide pair. Knowing that the transversal force from an infinite string on the junction can be written $f_i = f_{i+} + f_{i-} = Z_i(v_{i+} - v_{i-})$ (Appendix A) and combining this with equation 3.4 we get that $\sum_{i=1}^{N} Z_i(v_{i+} - v_{i-}) = 0$ which ultimately means that

$$2\sum_{i=1}^{N} Z_i v_{i+} = \sum_{i=1}^{N} Z_i(v_{i+} + v_{i-}) = \sum_{i=1}^{N} Z_i v_j \tag{3.5}$$

giving equations 3.6.

$$\begin{cases} v_{i-} = v_j - v_{i+} \\ v_j = 2\dfrac{\sum_{i=1}^{N} Z_i v_{i+}}{\sum_{i=1}^{N} Z_i} \end{cases} \tag{3.6}$$

Now, these are the equations that will prove usable to design the waveguide mesh. Connecting scattering junctions with waveguide pairs only 1 unit delay long we can create a two dimensional mesh using 4 pairs connected to every junction or a three dimensional mesh by connecting 6 pairs (see figure 3.3 and 3.4). That these constructs do indeed simulate the wave equation is proven in 3.3.2 where the equations obtained are compared to the Finite Difference Method. However, they do not provide the exact band limited simulation of the equation as every point of a real wave can be seen as a point source that spreads equally in every direction according to Huygens principle, in the waveguide mesh there are only a limited number of directions to choose from. The effects of this are analyzed in section 3.3.4 and section 3.3.5 contains suggestions on how to improve the performance.
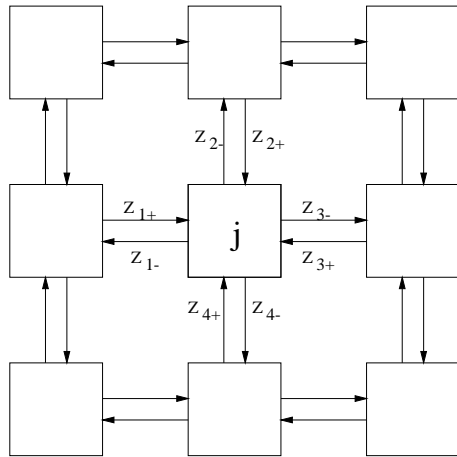
Figure 3.3: A rectangular two dimensional waveguide mesh
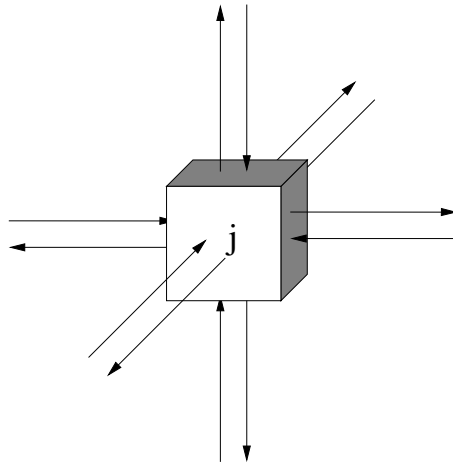
Figure 3.4: A rectangular three dimensional waveguide mesh element.

Also, an important note to make is that it takes two timesteps for the response of any interaction with the mesh to arrive back at the same junction. That is; the transferfunction of the mesh is a function of z^{-2} and therefore symmetric, so the frequency response above $0.25f_s$ is mirrored. This is illustrated by the fourier transform of a simulation of a circular mesh excited by an impulse in figure 3.9.

3.3.2   A comparison to the Finite Difference Method

It can be proven that the waveguide solution is equivalent to solving the wave equation using the Finite Difference Method. Here a proof is presented for the two dimensional rectangular waveguide mesh.

As stated in equation 3.5 the following relations apply (defining $v_{j,i}$ as the velocity of the junction at the other end of waveguide pair i from v_j)

13

$$v_j(n-1) = \frac{2}{N} \sum_{i=1}^{N} v_{i-}(n) \tag{3.7}$$

$$v_j(n+1) = \frac{2}{N} \sum_{i=1}^{N} v_{i+}(n) = \frac{2}{N} \sum_{i=1}^{N} \{v_{j,i}(n) - v_{i-}(n)\} \tag{3.8}$$

That is; the state of the junction last timestep can be found from the outgoing waves and the state to come can be calculated from the incoming waves if and only if the wave impedances of the wave guides connected to the junction are equal. Adding 3.7 and 3.8 together we get

$$v_j(n+1) + v_j(n-1) = \frac{2}{N} \sum_{i=1}^{N} v_{j,i}(n) \tag{3.9}$$

Discretising the wave equation $\frac{1}{c^2} \frac{\partial^2 v}{\partial t^2} = \frac{\partial^2 v}{\partial x^2} + \frac{\partial^2 v}{\partial y^2}$ using the Finite Difference Method with the time difference T and the membrane divided into sections of width X and height Y at timestep n, in section (a,b) of the membrane we get

$$\begin{aligned}
\tfrac{1}{c^2} \{ v(nT + T, aX, bY) - 2v(nT, aX, bY) + v(nT - T, aX, bY) \} = \\
v(nT, aX + X, bY) - 2v(nT, aX, bY) + v(nT, aX - X, bY) + \\
v(nT, aX, bY + Y) - 2v(nT, aX, bY) + v(nT, aX, bY - Y)
\end{aligned} \tag{3.10}$$

In comparing 3.10 to 3.9 (using figure 3.3) it is easily deduced that by setting T=1 and $c^2 = 0.5$ the two equations are interchangeable. The proof can be extended to N dimensions by extending the FDM formula and see how this corresponds to the two waveguide pairs added. For a rectilinear N dimensional mesh $c^2 = 1/N$.

3.3.3 Dispersion of a two dimensional rectangular waveguide mesh

The proof is an adoption of the proof presented for a triangular waveguide mesh by Fontana and Rocchesso in [7].

The following equation is the explicit expression of equation 3.9 at timeslot n with the same nomenclature as in equation 3.10.

$$\begin{aligned}
v_j(nT+T, aX, bY) + v_j(nT-T, aX, bY) = \quad & \tfrac{1}{2}v_j(nT, aX + X, bY) + \tfrac{1}{2}v_j(nT, aX - X, bY) + \\
& \tfrac{1}{2}v_j(nT, aX, bY + Y) + \tfrac{1}{2}v_j(nT, aX, bY - Y)
\end{aligned} \tag{3.11}$$

Calculating the two dimensional spatial Fourier transform of this expression we get

14
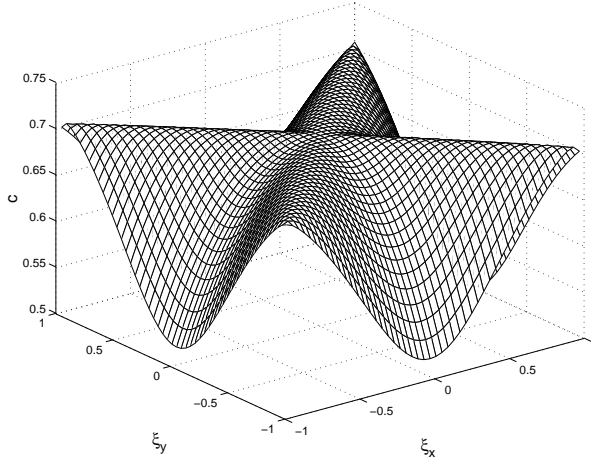
Figure 3.5: The speed of propagation of a wave in a rectangular mesh as a function of the spatial frequency.

$$V_j(nT + T, \xi_x, \xi_y) + V_j(nT - T, \xi_x, \xi_y) = bV_j(nT, \xi_x, \xi_y) \qquad (3.12)$$

with

$$b = \cos 2\pi \xi_x X + \cos 2\pi \xi_y Y$$

(Using the shift theorem $v(x - a) \supset e^{-2\pi j a \xi} V(\xi)$ and then Eulers equation $\cos \phi = \frac{e^{j\phi} + e^{-j\phi}}{2}$). Identifying equation 3.12 as a difference equation $V_j(n + 1) + V_j(n - 1) = bV_j(n)$ it can then be solved. The homogenous solution to the difference equation is $V_j(n) = C |r|^n \sin(n\theta + \varphi)$ where C and φ are not dependant on the frequency decided by the initial conditions and $r = \frac{b^2}{2} \pm j\frac{1}{2}\sqrt{4 - b^2}$, $|r| = 1$ and $\theta = \arctan \frac{\sqrt{4-b^2}}{b}$. Knowing that for a freely moving wave the angular frequency $\omega = 2\pi f = 2\pi c\sqrt{\xi_x^2 + \xi_y^2}$ and $t = Tn$, setting $\omega = \theta$ yields the following result

$$c(\xi_x, \xi_y) = \frac{1}{2\pi T \sqrt{\xi_x^2 + \xi_y^2}} \arctan \frac{\sqrt{4 - b^2}}{b} \qquad (3.13)$$

.

which is depicted with $T = 1$ in figure 3.5. At long wavelengths the speed of propagation is $c = \frac{1}{\sqrt{2}}$ as stated in 3.3.2, but as wavelengths get shorter speed of propagation becomes dependant on the direction of propagation. The rectangular mesh retains its speed of propagation in diagonal directions but waves travelling either horizontally or vertically will be slowed with a factor of up to $\frac{1}{\sqrt{2}}$ for short wavelengths. The analysis can be extended to N dimensions by symmetry.

15
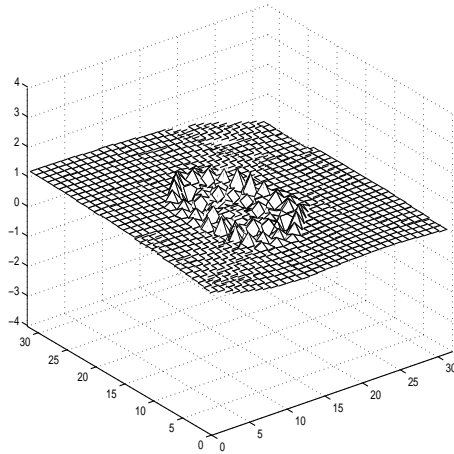
Figure 3.6: An impulse propagating from the center of a circular membrane.

3.3.4 A simulation of an ideal circular membrane

A series of simulations of a circular membrane was done to verify the validity of the formulas presented in 3.3.2. A corral of very high wave impedance was drawn into a quadratic mesh. The diameter of the corralle was varied between 15 and 120 units including the rim. The membrane was initially excited with an impulse at the center and then a number of time steps proportional to the diameter was simulated (10000 for a diameter of 15). For each time step the center node was sampled. The results were then transformed into the frequency domain and the fundamental frequency of the signal was identified. Instead of considering a larger diameter as a larger membrane it was assumed to be an oversampled version of the same membrane. The frequencies in table 3.1 have been scaled according to the first eigenfrequency of the ideal circular membrane. The fundamental frequency of the ideal membrane is the first eigenvalue of the solutions, which are the Bessel functions.

$$f_{01} = \frac{2.4048c}{\pi d} \tag{3.14}$$

The simulation of the ideal membrane is supposed to have a low frequency propagational speed $c = 2^{-0.5}$. In figure 3.7 the speed of propagation on membranes of different sizes calculated from the diameter of the membrane and the calculated fundamental frequency according to the relation 3.14 is shown.

Note that the frequencies of the simulation of the membrane with diameter 30 deviates distinctly from the general behavior by being slightly higher, I have no explanation for this.

3.3.5 Methods for correcting the dispersion

Most suggested methods for correcting the dispersion use these two steps:

16

Table 3.1: A comparison between the first resonant frequencies of a simulated membrane and the ideal solution, normalized by the theoretically ideal f_{01}.

Circle diameter	Simulated steps	f_{01}	f_{11}	f_{02}
15	10000	1.000	1.585	2.273
30	20000	1.003	1.596	2.295
45	30000	1.000	1.588	2.287
60	40000	1.000	1.591	2.289
75	50000	1.000	1.594	2.289
90	60000	1.000	1.594	2.292
105	70000	1.000	1.594	2.298
120	80000	1.000	1.594	2.295
Ideal	N/A	1.000	1.593	2.295
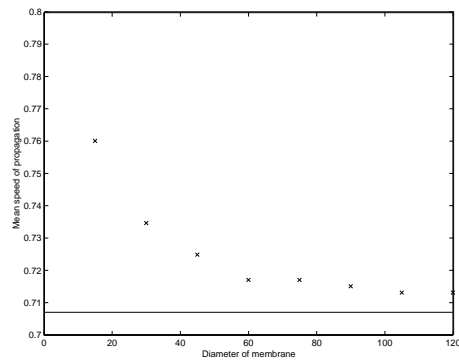
Figure 3.7: The mean speed of propagation on a simulated membrane for different sizes of the mesh (the line marked is $c = 2^{-0.5}$, predicted for low frequencies in section 3.3.2).
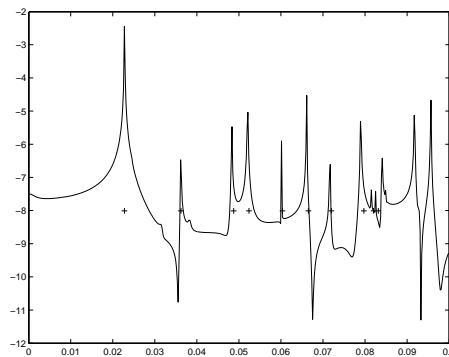
Figure 3.8: The resonances of a simulated membrane with the first 8 theoretical resonances, mapped to the simulations fundamental frequency, marked as crosses.

17
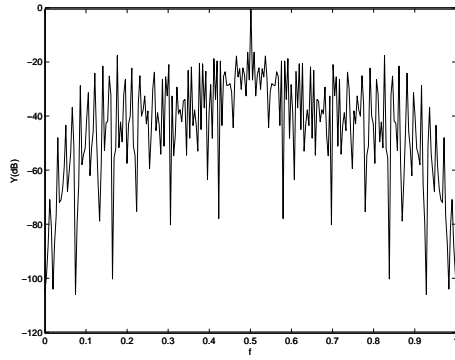
Figure 3.9: The full frequency spectrum of a circular membrane simulation.
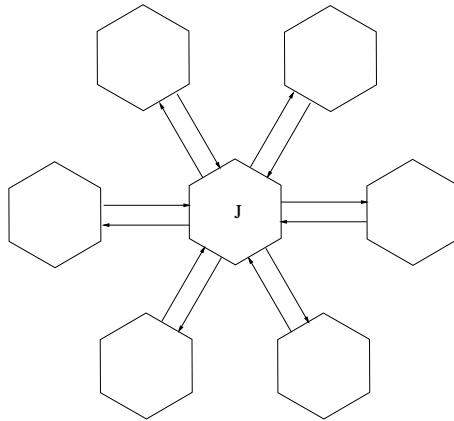
Figure 3.10: Improving the waveguide mesh with 6 connections.

1. Correcting the directional dependency of the dispersion.

2. Correcting the dispersion with a frequency dependent fractional delay.

The first step can be dealt with with a number of methods, the conceptually most easy being plain oversampling of the mesh to move the desired frequency range into the low frequency domain (see figure 3.5) where the dispersion is lower. Oversampling also automatically deals with step 2. This, however, is a computationally expensive as well as memory hungry method and it has been proven that using a more complex mesh is often more efficient. Two methods for this is presented here.

In [7] Fontana and Rocchesso suggest using a triangular mesh as illustrated in figure 3.10 because of the improvement of lowered directional dependency of the dispersion. Inserting equation 3.15 into equation 3.13 gives the propagation speed for this method depicted in figure 3.11.

$$b = \frac{2}{3}\cos(2\pi\xi_x X) + \frac{2}{3}\cos\left(2\pi\left[\frac{1}{2}\xi_x X + \frac{\sqrt{3}}{2}\xi_y Y\right]\right) + \frac{2}{3}\cos\left(2\pi\left[\frac{1}{2}\xi_x X - \frac{\sqrt{3}}{2}\xi_y c_y Y\right]\right)$$
$$(3.15)$$

18
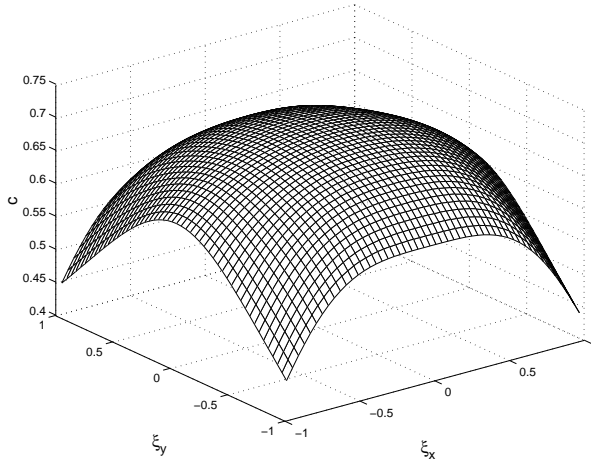
Figure 3.11: The speed of propagation in a triangular membrane as a function of the spatial frequency.

Lauri Savioja and Vesa Välimäki [8][9] have proposed an 8 connection waveguide mesh with a twist to improve the directional dispersion.Their method named deinterpolation uses the four surrounding junctions of the diagonal waveguides to interpolate the value of a virtual point at a unit distance from the junction, instead of taking the value leaving the diagonally opposite junction at a distance $\sqrt{2}$, see figure 3.12. The value of the virtual point can be calculated by linear interpolation according to $v_p = \frac{1}{2}v_{diagonal} + \frac{\sqrt{2}-1}{2}\left(v_{above} + v_{right}\right) + \frac{3-2\sqrt{2}}{2}v_j$ with labelling taken from the directions in figure 3.12(b).

Inserting equation 3.16 into equation 3.13 gives the propagation speed for this method depicted in figure 3.13.

$$b = \frac{1}{2}\left(\sqrt{2}\left[\cos(2\pi\xi_x X) + \cos(2\pi\xi_y Y)\right] + \frac{1}{2}\left[\cos(2\pi(\xi_x + \xi_y)X) + \cos(2\pi(\xi_x - \xi_y)Y)\right] + \frac{6 - 4\sqrt{2}}{2}\right)$$

(3.16)

 The next step is to correct the frequency dependence of the speed of propagation. As the spatial dependence has been reduced this can be considered in the temporal domain. To do this an allpass filter can be introduced at every junction to change the phase of the incoming waves and thereby create a phase change of $\phi(f)$ (rad) each step that would change the the speed of propagation of a wave with frequency f to

$$c = \left(\frac{1}{c_o} - \frac{\phi}{2\pi f}\right)^{-1}$$

(3.17)

As the phase delay is $180°$ at $0.5F_s$ a filter removing this frequency should be used in conjuction. The first order allpass filter is

$$H(z) = \frac{z^{-1} + \lambda}{1 + \lambda z^{-1}}$$

(3.18)

19
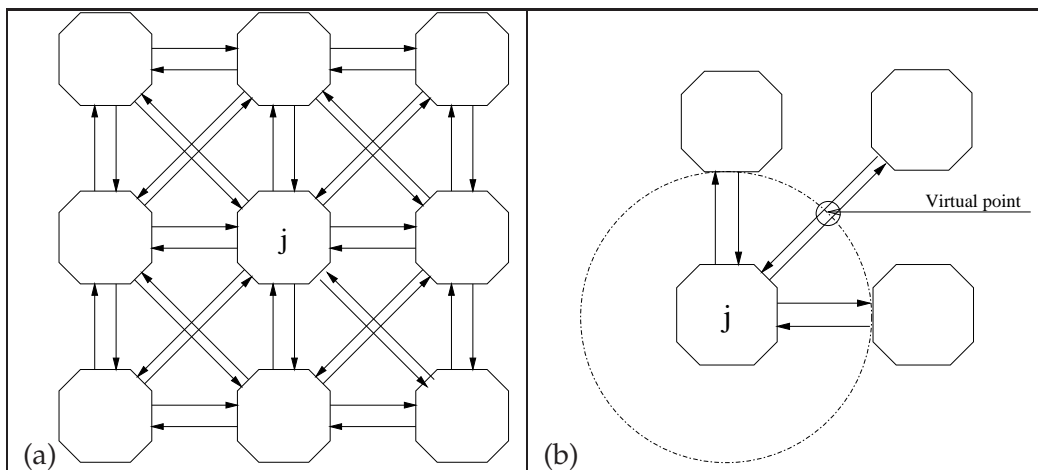
Figure 3.12: (a) Improving the wave guide mesh with 8 connections. (b) Further improvement with deinterpolation
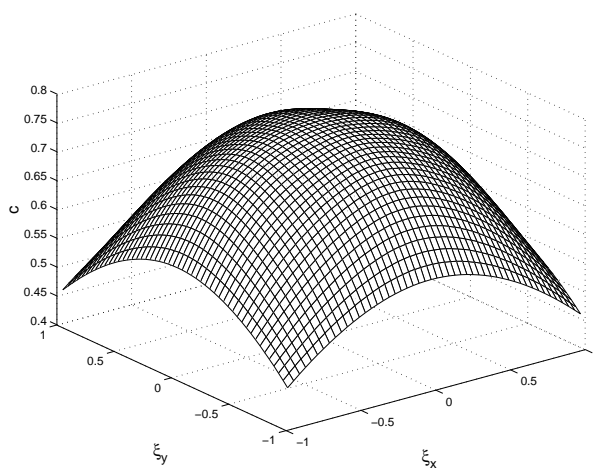
Figure 3.13: The speed of propagation in a deinterpolated membrane as a function of the spatial frequency.

In [8] a value of $\lambda = -0.1757$ is proposed to compensate the dispersion of their 8 connection deinterpolated mesh. This yields a relative frequency error, $\frac{c(\xi_x, \xi_y) - c(0,0)}{c(0,0)}$, of less than 1% up to 44% of the bandwidth, that is; 88% of the bandwidth of interest. In [17] Dattorro describes the use of the allpass filter as a fractional delay and gives the following relation

$$\lambda = \frac{1 - \Delta}{1 + \Delta}, \Delta \in [0,1]$$

3.4 Introducing damping in the model

3.4.1 Propagational damping

Introducing damping in the waveguide mesh is quite straight forward. The simplest of solutions is to multiply all outgoing velocities with a damping factor λ to achieve exponential decay everywhere according to $e^{-n \ln \lambda}$ where $n = F_s t$ is the timeslot. This yields a frequency independent damping. The relation between the damping factor and the time at which $60\, dB$ damping is reached is

$$\lambda = \left(\frac{1}{1000} \right)^{\frac{1}{F_s T_{60}}} \tag{3.19}$$

Introducing frequency dependent propagational damping is done in the same manner and the calculation of the damped membrane can be written as

$$v_- = \frac{B(z)}{A(z)}(v_j - v_+)$$

that is both FIR and IIR filters can be implemented by keeping a history of old meshes. There is a mechanism at work here that must be considered though, that can ultimately defeat the purpose of the filter and change the behavior entirely, and that is the phase delay of the filter as discussed in section 3.3.5. That means that the phase delay has to be compensated for or the speed of propagation will be warped.

Filtering does, of course, mean a considerable increase in processing load as well as memory use as $N + M$ copies of the velocities have to be stored where N and M are the orders of B and A respectively.

3.4.2 Modeling a stiff membrane

In section 3.3.5 allpass filtering to compensate for dispersion was suggested. The propagation speed of a free wave traveling on a stiff membrane was calculated in 2.3.2 (equation 2.4). This equation suggests that the speed of propagation increases with frequency so the same filter used in 3.3.5 (equation 3.18) can be used to compensate the dispersion and raise the speed of propagation of high frequencies. Other methods

21
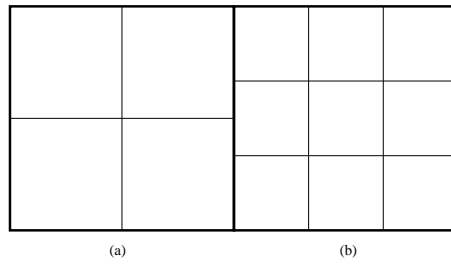
Figure 3.14: Two 2D meshes connected with the propagation speed of (a) $3/2$ of (b).

available to create for frequency dependent dispersion, like Lagrange interpolation, are available in [11].

3.5 Connecting waveguides

This section only covers rectangular waveguide meshes. It is important to note that only meshes with the same quantities propagating thru them can be connected in this way.

3.5.1 Connecting two 2-dimensional meshes

Connecting two 2D meshes at some edge has obvious applications. In this section I will deal with connecting two surfaces with different speeds of propagation and therefore probably different wave impedances. Both connected sides have the same length and the relation between them is N junctions for (a) to M junctions for (b) giving the relation $c_a = \frac{M}{N} c_b$. The difference of wave impedance is the easy part to deal with as it involves using the usual relations to calculate the reflections from the junctions (equation 3.6). The problem is converting the edge of the finer mesh to that of the coarser and vice versa. This problem is summarized as follows:

- When moving from a high resolution to a low resolution (low to high propagational speed) mesh the outgoing waveguides contain additional spatial high frequency information that must be filtered out before resampling, otherwise spatial high frequency folding occurs.

- When moving from a low resolution to a high resolution (high to low propagational speed) mesh the outgoing waveguides contain less spatial high frequency information so the signal has to be resampled to avoid aliasing.

The simplest approach is this: For every update, the outgoing waveguides from each of the interface lines are interpolated to the number of incoming waveguides, that is N outgoing waveguides from (a) are transformed into M incoming waveguides to (b) and vice versa. The calculated outgoing waveguides from (b) are then transformed back

22
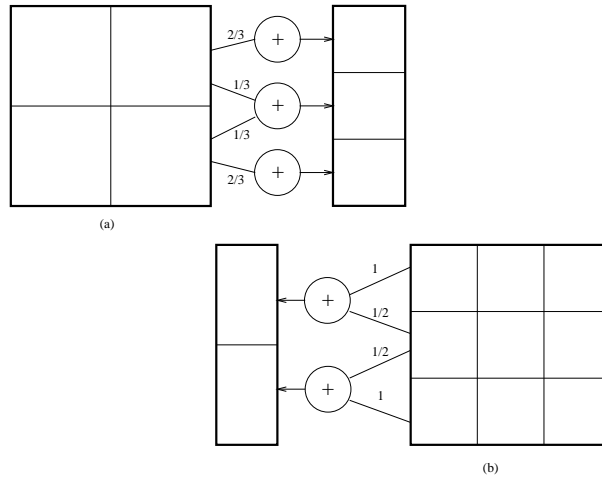
Figure 3.15: A simple conversion between the two meshes in figure 3.14.

into N incoming waveguides of (a). The general method here is to add a weighted sum of all the outgoing waveguides on the interface to get the interpolated waveguides

$$v_{interp,i-} = \sum_{j=1}^{N} a_{i,j} v_{j-}$$

where $i \in [1..M]$. An interpolating FIR filter can be used to interpolate the waveguides spatially, and by using a lowpass filter folding of high spatial frequencies when going from a slow-moving (high spatial resolution) to a fast-moving (low spatial resolution) can be avoided. This, however adds the problem of no longer preserving the sum of all velocities, that is a wave crossing the interface several time might be amplified or attenuated every time leading to some frequencies decaying exponentially while others grow exponentially leading to a diverging signal. An easy way to make the system lossless is using the scheme used in figure 3.15. The coefficients are chosen so that $a_{i,j}$ is the factor of how much of i covers j. This way the energy of the two meshes is preserved but folding and aliasing becomes an issue. The method is especially time efficient when converting between interfaces of almost the same size.

Another method is using the same grid size on both meshes but using fractional delays on the mesh with lower propagational speed. This can be done using the FIR Lagrange interpolator of order N whose coeffients can be calculated according to [11] as

$$h(n) = \prod_{k=0, k \neq n}^{N} \frac{D-k}{n-k}, n \in [0..N]$$

3.5.2 Connecting two 3D meshes

The concepts of 3.5.1 can easily be extended into connecting two 3-dimensional meshes at a surface interface. Using vector algebra extending the conversion vector a_i is a

23

matter of calculating $a_{ij} = a_i \cdot a_j^T$ where (i,j) is the position of the outgoing waveguide.

3.5.3 Connecting a 2D and a 3D mesh

To do this the two-dimensional mesh has to have one (if connected on the surface of the three dimensional mesh) or two waveguide pairs added to every junction essentially making it a one layer three-dimensional mesh. This can be inserted anywhere in the three-dimensional mesh by replacing a "chisel" of junctions with the 2-dimensional mesh.

3.6 Connecting systems with different quantities.

3.6.1 The loaded junction.

Suppose that a junction in the mesh is acted upon by an external force f_{ext}, then equation 3.4 would have to be altered to:

$$\sum_{i=1}^{N} f_i = f_{ext} \tag{3.20}$$

giving a new expression to calculate the junction velocity

$$v_j = \frac{2\sum_{i=1}^{N} Z_i v_{i+} - f_{ext}}{\sum_{i=1}^{N} Z_i} \tag{3.21}$$

Adding such an external force is one way to add an excitation of the mesh in a point. The force f_{ext} can be a function of physical properties of the mesh or, as a simplification, a function of time can be used to inject a signal into the meshes (for example, a vocal sample into a reverbating room simulation). If the signal is post warped to compensate for the frequency dispersion, it is essential to prewarp f_{ext}.

3.6.2 Connecting two waveguide meshes with different quantities.

Assuming two junctions effect on each other can be formulated as an external force that is $f_{(a)} = f_{(a)}(v_{j(b)})$ and $f_{(b)} = f_{(b)}(v_{j(a)})$ the loaded junction (equation 3.21) can be used to connect two systems. This method will be used to connect air and drum heads in the drum model.

3.6.3 Connecting an exciter to the mesh

The article [13] describes a model of the wave digital hammer based upon wave digital filtering [14]. The term hammer is used because the model was originally intended to
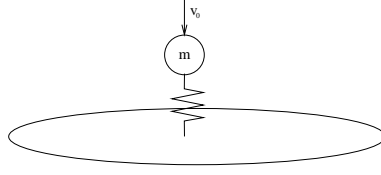
Figure 3.16: A digital hammer exciting the membrane

model piano hammers. The filter is made by setting up force equations modeling the exciter. It is modeled as a mass and a nonlinear spring where the spring is used to approximate the elastic properties of the head. The mass is excited at $t = 0$ with an impulse giving it the initial speed v_0.

$$
\begin{cases}
f_m = m\frac{\partial v_m}{\partial t} - mv_o\delta(t) \\
f_k = k(x_k)x_k \\
f = f_k + f_m \\
v = v_k + v_m
\end{cases}
\tag{3.22}
$$

Where v is the membrane velocity. The following nonlinear spring constant is suggested in literature:

$$
k(x_k) = \begin{cases}
k_o x_k^p & x_k > 0, \ p \geq 0 \\
0 & x_k < 0
\end{cases}
$$

Connected masses with linear springs have been used in [7] to model air loading of membranes. The system 3.22 is transformed into the wave domain using Laplace transform and then $F(s)$ and $V(s)$ is substituted by the wave variables $V_{in}(s)$ and $V_{out}(s)$ related as $F(s) = R_h(V_{in}(s) - V_{out}(s))$, $V(s) = V_{in}(s) + V_{out}(s)$.

$$
V(s) = V_k(s) + V_m(s) = \frac{s}{k}F_k(s) + \frac{1}{ms}F_m(s) + \frac{v_0}{s}
$$

$$
V_{out}(s) = \frac{s^2 - (k/R_h)s + k/m}{s^2 + (k/R_h)s + k/m}V_{in}(s) + \frac{v_0 k/R_h}{s^2 + (k/R_h)s + k/m}
$$

These relations are then discretised using the bilinear transform

$$
s \leftarrow \alpha\frac{1 - z^{-1}}{1 + z^{-1}}
$$

where α is generally chosen to be $2F_s$. This yields an allpass filter parallel to a transient impulse

$$
v_{out} = \frac{b0 + b1z^{-1} + z^{-2}}{1 + b1z^{-1} + b0z^{-2}}v_{in} + \frac{mkv_0 F_s}{T(mR_h\alpha^2 + mk\alpha + kR_h)}\left(\frac{1 + 2z^{-1} + z^{-2}}{1 + b1z^{-1} + b0z^{-2}}\right)
$$

25

where

$$b0 = \frac{mR_h\alpha^2 - mk\alpha + kR_h}{mR_h\alpha^2 + mk\alpha + kR_h}, \quad b1 = \frac{2(kR_h - mR_h\alpha^2)}{mR_h\alpha^2 + mk\alpha + kR_h}$$

As R_h is arbritrary [13] chooses it so that $b0 = 0$, making $v_{out}(n)$ a function of $v_{in}(n-1)$, and thereby possible to connect to a waveguide junction (i.e not a delay-free loop).

$$R_h = \frac{mk\alpha}{m\alpha^2 + k}$$

As $k = k(x_k)$ the next difficulty is tracking x_k to generate the current k. The method suggested in [13] is using

$$x_k = \frac{f_k}{k} = \frac{f_{in} + f_{out}}{k} = \frac{R_h(v_{in} - v_{out})}{k} \tag{3.23}$$

This way, $x_k(n-1)$ can be calculated as all the right hand variables of the last timestep are known. Calculating $x_k(n)$ is harder but possible if all incoming waves to the junction are known, v_{in} and k are then functions of x_k and x_k is implicitly defined by equation 3.23 and 3.6.

4   Using waveguides to model a drum

A series of measurements of real tom tom drums have been made and are described in appendix C. The parameters of the 14″ tom tom are used as basis for the modeling of a tom tom drum. The results of the simulations are then compared to recordings of the real counterpart.

4.1   Modeling drum heads

The parameters of the drumheads are chosen to approximate the tom toms used in Appendix C.

A superficial density of $\sigma = 0.5 kg/m^2$ is assumed for all drum heads. The measured speed of propagation is $c_b = 53 m/s$ for the battering head and $c_r = 75 m/s$ for the resonant head. The diameter of the heads is $d = 0.35m$. Selecting a sampling frequency $F_s = 22050 Hz$ a mesh resolution can be calculated as

$$\triangle s = \frac{\sqrt{2}c}{F_s} \tag{4.1}$$

and therefore the number of nodes of the diameter of the drum head, $D = \frac{d}{\triangle s}$, yields $D_b \approx 103$ and $D_r \approx 73$.

The impedance (appendix A) of a membranes is $Z = \sigma c$ relating transversal velocity to transversal membrane tension. In [16, 15] a more useful impedance is selected relating the transversal velocity to the forces exerted by one element of the mesh. This makes the impedance also a function of mesh characteristics. As the element is rectangular multiplying the impedance with $\triangle s/2$ gives the force exerted by a velocity waveguide pair $Z_{mesh} = \frac{\sigma c^2}{\sqrt{2}F_s}$, regardless of traveling direction. It is divided by two because it is shared between two elements. In this particular case $Z_{meshb} = 0.045 kg/s$ and $Z_{meshr} = 0.09 kg/s$

4.2   Modeling enclosed air

The air enclosed in the tom tom drum has the form of a cylinder with a height of $h = 0.25m$ and a diameter of $d = 0.35m$. The mesh resolution in 3D can be calculated as

$$\triangle s = \frac{\sqrt{3}c}{F_s} \tag{4.2}$$

Using $c = 340\,m/s$ the number of nodes of the height becomes $H_a \approx 9$ and the diameter $D_a \approx 13$. The volume density of air is $\rho = 1.19 kg/m^3$ giving an impedance

$Z_{air} = 410 kg/m^2 s$ relating particle velocity to pressure. As the property of interest is air pressure deviataions p_a pressure waves are chosen as the property traversing the wave guide mesh. This gives immediate access to the junction pressure, p_j.

Summing wave velocities to zero at the junction leads to the admittance, $Y_{air} = Z_{air}^{-1} = 0.00228 m^2 s/kg$, replacing impedance in the junction equation. The boundary condition of air against a rigid wall, equation 2.1, gives that $p_- = p_+$ in wave guide pairs connecting to the boundary.

4.3 Modeling the drum shell

The drum shell supports several types of waves (chapter 2) with different speeds of propagation and different coupling to its surroundings. Here the drum shell will be considered to be a rigid and heavy boundary for the membranes and air. A more detailed model would use several interconnected cylindrical 2d wave guides to model interaction between different wave types.

4.4 A model of the drum stick

Recordings of the force interaction between the drum head and the force transducer were done at several locations on the head (appendix C). These were used as exciters of the drum model as defined by equation 3.21. The recordings were frequency limited to $F_s/4$.

4.5 Connecting the different parts of a drum

The different parts of the drum have different impedances and speed of propagation, leading to different mesh resolutions. The method of connecting meshes is described in chapter 3.5 and by defining compatible impedance relations the meshes can be connected using added interface waveguides to the boundary junctions as a useful special case of the equations 3.20 and 3.21.

4.5.1 Connecting the hammer to the membrane

The hammer described in section 3.6.3 or 4.4 can be directly attached to the membrane either using a waveguide pair or adding a force, equation 3.21, assuming the membrane impedance is chosen as Z_{mesh} in section 4.1.

4.5.2 Connecting the membranes to air

Membranes can be connected using the mesh dependent impedances stated in section 4.1 and 4.2. There are two important things to consider
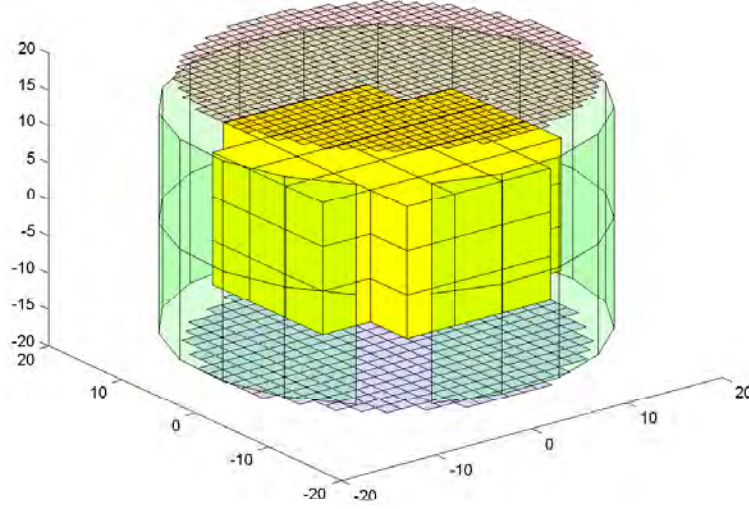
Figure 4.1: Waveguide parts of a drum.

- The position of the air relative the membrane matters. Incoming pressure waves from below the membrane give a positive contribution to the total external force while incoming velocity waves from above the membrane give a negative contribution. Assuming that A is the area of the membrane mesh element, $p^{above} = p_+^{above} + p_-^{above} = Z_{air}(v_-^{above} - v_+^{above})$ is the pressure from air above the membrane and $p^{below} = p_+^{below} + p_-^{below} = Z_{air}(v_+^{below} - v_-^{below})$ from below leads to the following reflection relations

$$v_- = v_j - v_+ = \frac{2\sum_{i=1}^N Z_i v_{i+} - 2Ap_+^{above} + 2Ap_+^{below}}{\sum_{i=1}^N Z_i + 2Z_{air}A} - v_+$$

$$\begin{cases} p_-^{below} = p_+^{below} - Z_{air}v_j \\ p_-^{above} = p_+^{above} + Z_{air}v_j \end{cases}$$

- As mesh resolution is different between the different meshes each boundary waveguide has to be spread out to all junctions it overlaps and be scaled down according to how much area the destination element occupies of the source element (section 3.5.1 & 3.5.2).

Point two was modified slightly to improve computability. Every air cell was connected to a corresponding square of the membrane leaving junctions at the edges of the membrane unconnected.

4.6 Recording the sound from the drum

To correctly simulate the external air loading of the membranes and to have recording point corresponding to the microphone placement in appendix C (figure C.2) an anechoic chamber surrounding the drum is simulated. The chamber is chosen to be cubic with $2m$ sides . Using equation 4.2 the chamber mesh needs to be of size $H_{ch} = 75$. Anechoic boundary conditions are approximately simulated by removing reflections from junctions at the boundary.

The drum is placed with the center of the battering head at the center of the box at coordinate $(38, 38, 38)$. The microphone is placed at coordinate $(12, 38, 64)$ approximating the position in appendix C (figure C.2)

4.7 Results from simulating the tom tom drum

4.7.1 Simulations of drum parts

The following two drum configurations were simulated.

- Battering head, air and drumshell.

- Battering head, resonant head, air and drum shell.

The battering head was excited with the recorded hammer force from appendix C at the center and 2/3 of the radius of the drum head matching position 1 and position 3 (figure C.3). The connection between drum head and air described in 4.5.2 proved to have a flaw that made it unsuitable with considerable oversampling of the mesh. The large difference in mesh resolution between drum head and air, 103 junctions in diameter compared to 11, makes a lot of membrane junctions connected to one air node act as a spatial low pass filter quickly filtering out all high frequency content from the membrane but the lowest resonances. Instead each interfacing air junction was connected to just one membrane junction. This yields a full frequency spectrum although the higher frequencies are most certainly not correct. Analysis of samples from the real membrane shows that the resonances die off quickly between 400Hz and 1000Hz. Passing the simulations thru a 4th order Butterworth filter with a 400Hz cut off frequency gave a realistic sounding tail of the sound indicating that high frequency damping factors are missing in this model.

4.7.2 A comparison of frequencies and decay times

The frequency of the lowest resonance of both simulated drums matches the measured resonance in appendix C very well. The following resonances are generally lower than their measured counterparts. The frequencies of the drum head are matched to eigenfrequencies of the ideal membrane in table 4.1.

Table 4.1: Resonances of the one head tom tom drum.

Head of the drum	f_{01} (Hz)	f_{11} (Hz)	f_{02} (Hz)
Battering head	89	162	233
Measured battering head	90	177	260

Figure 4.2: Resonances of a one head tom tom hit at (left) center and (right) 2/3 of radius. Dotted line is recorded, whole line is simulated.

When simulating the two headed tom tom drum the resonances created by the resonant skin were hard to isolate from the shifted resonances of the battering skin. The frequencies are matched to eigenfrequencies of the ideal membrane in table 4.2.

Table 4.2: Resonances of the two head tom tom drum

Head of the drum	f_{01} (Hz)	f_{11} (Hz)	f_{02} (Hz)
Battering head	114	165	246
Measured battering head	116	176	260
Resonant head	177?	225?	339?
Measured resonant head	?	?	373

The decay rate of all the simulated membranes is identical at approximately $20dB/s$. Analysis of the recordings from appendix C show that the drum has a decay rate of $15 - 20dB/s$ in the tail of the sound. Drums hit at the center, though, seem to have a faster initial decay than hits further off center. This quality is not present in the simulations and will therefore be attributed to phenomena like increased membrane tension or possibly air turbulence.
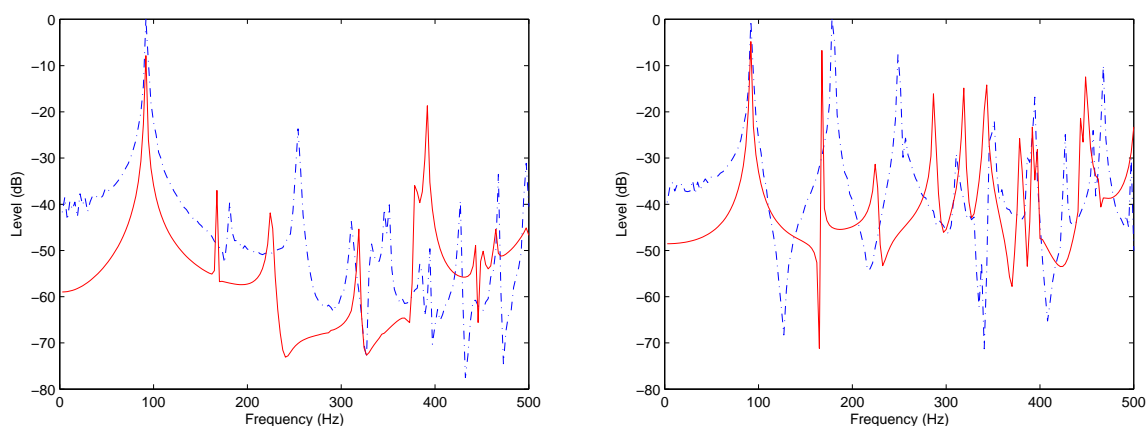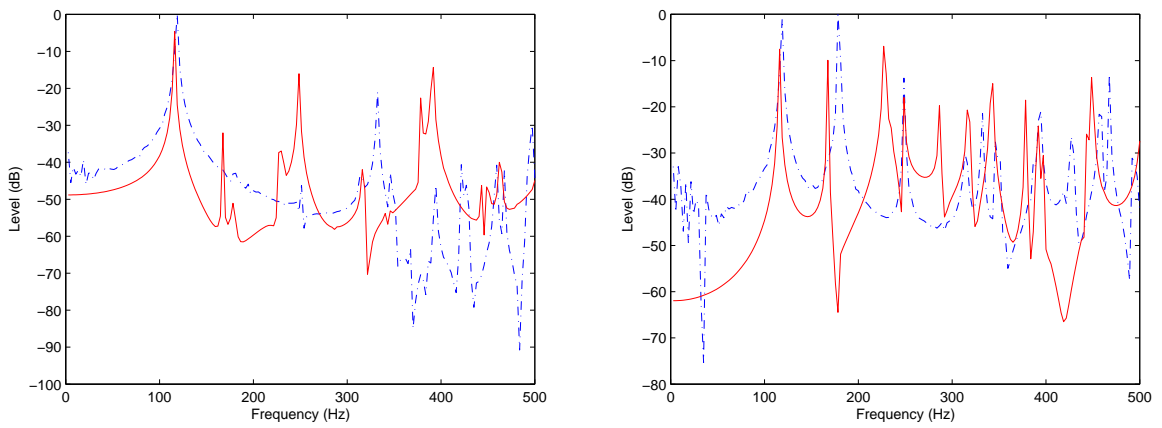
Figure 4.3: Resonances of a two head tom tom hit at (left) center and (right) 2/3 of radius. Dotted line is recorded, whole line is simulated.

5 Conclusions

5.1 Quality of results

The simple model used in this project does have recognisable properties from a real tom tom drum but is unconvincingly static sounding, probably because detailed frequency dependent damping mechanisms are missing. The most important part of a drum sound is the attack which is a weak part of this model due to lacking a mechanism for varying membrane tension or a detailed physical model of the strike of a drumstick.

5.2 Simulation complexity

The calculation complexity of the N-dimensional ($N > 1$) waveguide mesh is $O(F_s^N)$ and $O(d^N)$ where F_s is the sampling frequency and d is a general dimension of the simulated object. This means that oversampling or increasing the size of the drum is very expensive. Although the digital waveguide method is efficient compared to finite difference methods full frequency real time simulation of real size drums is currently a task for a super computer requiring several billion floating point operations per second.

5.3 Further research

Detailed damping. Frequency dependent air damping and damping in drum head and the rim was ignored in the simulations done for this report. In a more detailed simulation where current flaws have been addressed such extensions would probably provide vastly extended realism.

Interaction with shell. This interaction was ignored in my simulations but as reported by drummers different materials give different sounds, partly because of varying diffusion of the sound waves in the enclosed air.

Air turbulence modeling. What are the effects of air turbulence on acoustics and how can the waveguide model be extended to model such effects?

A membrane with varying tension. This could be possible to realize either as inserting fractional delays between junctions and simulate observed tension variations or by extending the model beyond the wave equation and possibly simulating them using wave digital filtering as described in [18]

Appendix A Derivation of wave impedance

A.1 Deriving the transverse wave equation of an ideal string.

(This derivation is based on [4])

Assuming that the restoring force on the segment $[x, x + \triangle x]$ can be calculated as the difference between the transverse components of the tension K in the string and assuming that the displacement is small so that Taylor approximation can be used once to approximate the difference with linear interpolation and to approximate $\sin \theta$ with $\tan \theta = \frac{\partial y}{\partial x}$.

$$K_y = K \sin \Theta \approx K \tan \Theta = K \frac{\partial y}{\partial x} = f \tag{A.1}$$

$$\frac{\partial f}{\partial x} = \lim_{\triangle x \to 0} \frac{K \left(\frac{\partial y}{\partial x}(x + \triangle x) - \frac{\partial y}{\partial x}(x) \right)}{\triangle x} = K \frac{\partial^2 y}{\partial x^2} \tag{A.2}$$

Assuming $ds \approx dx$ for a sufficiently small dx so that the linear mass density at the segment can be written $\frac{\partial m}{\partial s} \approx \frac{\partial m}{\partial x} = \epsilon$. Then, applying Newton's second law of motion $f = ma$, we get

$$K \frac{\partial^2 y}{\partial x^2} = \frac{\partial f}{\partial x} = \frac{\partial}{\partial x} \left(m \frac{\partial^2 y}{\partial t^2} \right) = \epsilon \frac{\partial^2 y}{\partial t^2}$$

which can be written as

$$\frac{\partial^2 y}{\partial t^2} = c^2 \frac{\partial^2 y}{\partial x^2} \tag{A.3}$$

where $c = \sqrt{\frac{K}{\epsilon}}$. Differentiating A.1 twice with respect to t and A.2 with respect to x and then comparing it to A.3 differentiated with respect to x gives:
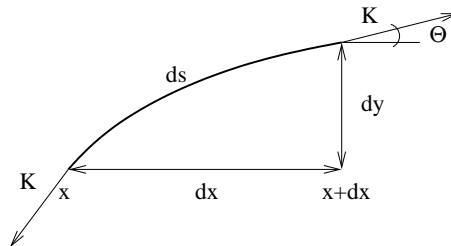

Figure A.1: The forces acting on a string with tension K

$$K\frac{\partial^2 f}{\partial x^2} = \epsilon\frac{\partial^2 f}{\partial t^2} \tag{A.4}$$

D'Alemberts solution to the wave equation states that $y = y_{right}(x - ct) + y_{left}(x + ct)$ and $f = f_{right}(x - ct) + f_{left}(x + ct)$

A.2   Derivation of the wave impedance of an infinite string

(This derivation is based on J.O Smith [12], page 432)

Starting from equation A.1 and inserting d'Alemberts solution we get

$$f = K\frac{\partial y}{\partial x} = K\left(\frac{\partial y_{right}}{\partial x}(x - ct) + \frac{\partial y_{left}}{\partial x}(x + ct)\right)$$

Then using the relations $\frac{\partial y_{right}}{\partial t}(x - ct) = -c\frac{\partial y_{right}}{\partial x}(x - ct)$, $\frac{\partial y_{left}}{\partial t}(x + ct) = c\frac{\partial y_{left}}{\partial x}(x + ct)$ and substituting $\frac{\partial y}{\partial t}$ with v.

$$f = f_{right} + f_{left} = \frac{K}{c}\left(v_{left} - v_{right}\right)$$

Defining $Z = K/c = \sqrt{K\epsilon} = \epsilon c$ as the wave impedance we get the relations

$$f_{right} = -Zv_{right}$$
$$f_{left} = Zv_{left}$$

J.O Smith defined f with an opposite sign to match the equations to waves in tubes but this is arbitrary.

A.3   The wave impedance in membranes and air

A wave impedance can also be defined for plane waves moving in membranes or gas. If the plane wave moves in the x direction the equations in section A.2 hold. For the isotropic membrane f is replaced with transversal force density of unit N/m and $Z = \sigma c$ where σ is the area density . For gas f is replaced with the gas pressure deviation p of unit N/m^2 and $Z = \rho c$ where ρ is the volume density.

Appendix B   Implementation in MATLAB

B.1   System requirements

This library makes use of 'structures' introduced in MATLAB 5 and it also uses functions from 'signal processing tool box'. 3D waveguides demand a lot of processing power as well as a internal memory, so to use these functions properly I recommend at least 512 Mbyte internal memory and a stable operating system like Windows XP, Mac OS X or Unix.

B.2   An overview of the function library

B.2.1   Structures of a waveguide mesh

field	description
dim	The dimension of the mesh (2 or 3).
sign	Sign of reflections from each junction.
zr	Wave impedance of the waveguide pair to the right.
zl	Wave impedance of the waveguide pair to the left.
zu	Wave impedance of the waveguide pair above (up).
zd	Wave impedance of the waveguide pair below (down).
ztot	The sum of the wave impedances divided by 2.
v	The junction velocity.
vr	The incoming waveguide from the right.
vl	The incoming waveguide from the left.
vu	The incoming waveguide from above (up).
vd	The incoming waveguide from below (down).

If dim=3 then the following variables are also defined

field	description
zi	Wave impedance of the waveguide pair on the back (in).
zo	Wave impedance of the waveguide pair on the front (out).
vi	The incoming waveguide from behind (inward).
vo	The incoming waveguide from front (outward).
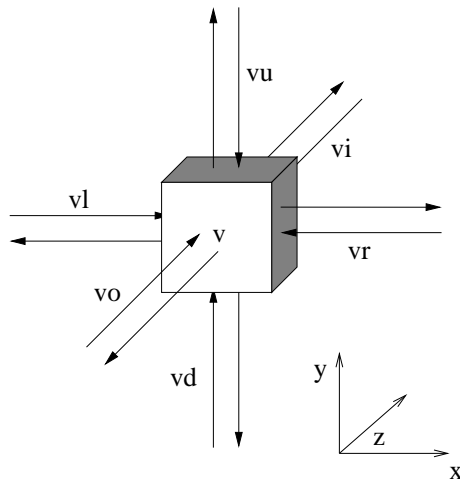
Figure B.1: The directions of the structure fields.

B.2.2   A typical core processing loop

```
% Initiate parameters of simulation
n_steps=44100;        % Length of simulation
fs=44100;             % Sampling frequency
t60=1.0;              % decaytime (s)
c=53;                 % velocity (m/s)
%   Calculate membrane size and center
dl=sqrt(2)*c*(1/fs);
diam=round(size/dl);
sx=diam+4;sy=diam+4;
cx=floor(sx/2);cy=floor(sy/2);
%   Design a circular membrane
e=make_guide(2,sx,sy,1,1);
e=make_cylinderxy(e,cx-round(diam/2),cy-round(diam/2),cx+round(diam
   /2),cy+round(diam/2),1,1,10000);
f=zeros(sx,sy);
%   Add artifical t60 damping
damp=(1/1000)^(1/(fs*t60));
e.ztot=e.ztot/damp;
%   Run the loop
for t=1:n_steps
    f(cx,cy)=hammer_force(t,e); % Generic hammer
    e=reflect2d(e,f);
    snd(t)=e.v(cx,cy);
end
```

B.3 Functions for creating and designing waveguide meshes

B.3.1 mesh=make_guide(dimension,x,y,z,init_impedance)

The functions creates a waveguide mesh structure of size $x \times y \times z$ described in 7.2.1. Dimension should be 2 for two dimensions and 3 for three dimensions.

```
function e=make_guide(n,x,y,z,r)
% e=make_guide(n,x,y,z,r)
% make_guide creates a waveguide mesh structure  of the size
% x,y [,z] of dimension 'n' (2 or 3)
% The mesh is then initialized with the impedance r

% Set the dimension.
  e.dim=n;
% Create sign of reflections
    e.sign=ones(x,y,z);
% Create the impedances.
  e.zr=r*ones(x,y,z);
  e.zl=e.zr;
  e.zu=e.zr;
  e.zd=e.zr;
% Calculate the sum of the impedances
  e.ztot=4*e.zr/2;
% Create the velocities.
  e.v=zeros(x,y,z);
  e.vr=e.v; e.vl=e.v;
  e.vu=e.v; e.vd=e.v;

  if (n==3)
    e.vi=e.v;   e.vo=e.v;
    e.zi=e.zr;  e.zo=e.zr;
    e.ztot=6*e.zr/2;
  end
```

B.3.2 mesh=make_cylinderxy(mesh,x0,y0,x1,y1,z0,z1,impedane)

The function creates an empty elliptical cylinder in the z direction.

```
function aa=make_cylinderxy(e,x0,y0,x1,y1,z0,z1,r)
% Draw a cylinder with impedance r in e
global aa;
aa=e;
[sx sy sz]=size(aa.v);
cx=((x1+x0)/2);    cy=((y1+y0)/2);
a2=((x1-x0)/2)^2; b2=((y1-y0)/2)^2;
% Draw a cylinder
oy=0;
```

```
for i=x0:x1
    xx=i-cx;
    yy=sqrt((1-(xx^2)/a2)*b2);
    step=sign(yy-oy);
    for z=z0:z1
        for ii=oy:step:yy
            wgplot(round(i),round(cy+ii),z,r);
            wgplot(round(i),round(cy-ii),z,r);
        end
        wgplot(round(i),round(cy+yy),z,r);
        wgplot(round(i),round(cy-yy),z,r);
        oy=yy;
    end
end

function wgplot(xx,yy,zz,r)
    global aa;
    aa.ztot(xx,yy,zz) = abs(r);
    aa.sign(xx,yy,zz) = sign(r);
```

B.3.3   mesh=make_membxy(mesh,x0,y0,x1,y1,z0,z1,impedance)

The function creates a solid elliptical cylinder in the z direction.

```
function aa=make_membxy(e,x0,y0,x1,y1,z0,z1,r)
% Draw a filled cylinder with impedance r in e
global aa;
aa=e;
[sx sy sz]=size(aa.v);
cx=((x1+x0)/2);    cy=((y1+y0)/2);
a2=((x1-x0)/2)^2; b2=((y1-y0)/2)^2;
% Draw a filled cylinder
for i=x0:x1
    xx=i-cx;
    yy=sqrt((1-(xx^2)/a2)*b2);
    ii=round(i);
    for jj=round(cy-yy):round(cy+yy)
        for z=z0:z1
            wgplot(ii,jj,z,r);
        end
    end
end

function wgplot(xx,yy,zz,r)
    global aa;
    aa.ztot(xx,yy,zz) = abs(r);
    aa.sign(xx,yy,zz) = sign(r);
```

B.3.4 matrix=make_circmaskxy(x,y,x0,y0,x1,y1)

This function creates matrices to mask out circular areas in other matrices

```
function aa=make_circmaskxy(x,y,x0,y0,x1,y1)
% Draw a cylinder with impedance r in e
aa=zeros(x,y);
cx=((x1+x0)/2);   cy=((y1+y0)/2);
a2=((x1-x0)/2)^2; b2=((y1-y0)/2)^2;

for i=x0:x1
    xx=i-cx;
    yy=sqrt((1-(xx^2)/a2)*b2);
    for jj=round(cy-yy):round(cy+yy)
        aa(round(i),jj)=1;
    end
end
```

B.4 Functions for manipulating a waveguide mesh

B.4.1 mesh=reflect2d(mesh,force)

The function calculates the new junction velocities and then the reflections in two dimensions.

```
function e=reflect2d(e,f)
% e=reflect2d(e,f)
% Calculate reflections of 2D Waveguide mesh e with added forces f
  [xm,ym,zm]=size(e.zl); % Determine size of structure
% Calculate junction velocity
  e.v = (e.zr.*e.vr+e.zl.*e.vl+e.zu.*e.vu+e.zd.*e.vd-0.5*f)./e.ztot;
% Calculate returning reflections
  vl_2=e.v-e.vr;vr_2=e.v-e.vl;vu_2=e.v-e.vd;
  vd_2=e.v-e.vu;
% Place reflection at correct positions
  vl_pad=zeros(1,ym,1);
  vu_pad=zeros(xm,1,1);
  e.vl = [vl_pad;vl_2(1:(xm-1),:,:)];
  e.vr = [vr_2(2:xm,:,:);vl_pad];
  e.vu = [vu_2(:,2:ym,:) vu_pad];
  e.vd = [vu_pad vd_2(:,1:(ym-1),:)];
```

B.4.2 mesh=reflect3d(mesh,force)

The function calculates the new junction velocities and then the reflections in three dimensions.

```
function e=reflect3d(e,f)
% e=reflect3d(e)
% Calculate reflections of 3D Waveguide mesh e with added forces f
  [xm,ym,zm]=size(e.zl);
% Calculate junction velocity
  e.v = (e.zr.*e.vr+e.zl.*e.vl+e.zu.*e.vu+e.zd.*e.vd+e.zo.*e.vo+e.zi
     .*e.vi-0.5*f)./e.ztot;
% Calculate returning reflections
  vl_2=e.v-e.sign.*e.vr;vr_2=e.v-e.sign.*e.vl;vu_2=e.v-e.sign.*e.vd;
  vd_2=e.v-e.sign.*e.vu;vi_2=e.v-e.sign.*e.vo;vo_2=e.v-e.sign.*e.vi;
% Place reflection at correct positions
  vl_pad=zeros(1,ym,zm);
  vu_pad=zeros(xm,1,zm);
  vo_pad=zeros(xm,ym,1);
  e.vo = cat(3,vo_pad,vo_2(:,:,1:(zm-1)));
  e.vi = cat(3,vi_2(:,:,2:zm),vo_pad);
  e.vl = [vl_pad;vl_2(1:(xm-1),:,:)];
  e.vr = [vr_2(2:xm,:,:);vl_pad];
  e.vu = [vu_2(:,2:ym,:) vu_pad];
  e.vd = [vu_pad vd_2(:,1:(ym-1),:)];
```

B.4.3   matrix=blowup(original_matrix,ratio)

Two versions of the routine used to enlarge a two dimensional junction matrix to match a mesh $ratio > 1$ times bigger. Blowup is described in section 4.5.2, blowup2 is described in section 4.7.2

```
function b=blowup(a,ratio)
    [x,y]=size(a);
  b=zeros(ratio*x,ratio*y);
   for i=1:ratio*x
       for j=1:ratio*y
           b(i,j)=b(i,j)+a(floor(1+(i-0.5)/ratio),floor(1+(j-0.5)/
              ratio));
       end
    end

function b=blowup2(a,ratio)
    [x,y]=size(a);
  b=zeros(ratio*x,ratio*y);
   for i=1:x
       for j=1:y
           b(floor(1+(i-0.5)*ratio),floor(1+(j-0.5)*ratio))=a(i,j);
       end
    end
```

B.4.4   matrix=blowdown(original_matrix,ratio)

Two versions of the routine used to shrink a two dimensional junction matrix to match a mesh $ratio < 1$ times bigger. Blowdown is described in section 4.5.2, blowdown2 is described in section 4.7.2

```
function b=blowdown(a,ratio)
    [x,y]=size(a);
    b=zeros(ratio*x,ratio*y);
    for i=1:x
        for j=1:y
            b(floor(1+(i-0.5)*ratio),floor(1+(j-0.5)*ratio))=b(floor
                (1+(i-0.5)*ratio),floor(1+(j-0.5)*ratio))+a(i,j);
        end
    end

function b=blowdown2(a,ratio)
    [x,y]=size(a);
    b=zeros(ratio*x,ratio*y);
    for i=1:ratio*x
        for j=1:ratio*y
            b(i,j)=a(floor(1+(i-0.5)/ratio),floor(1+(j-0.5)/ratio));
        end
    end
```

B.5   Simulating a one headed tom tom drum

The function returns $nsteps$ samples of the sound pressure level measured at the co-ordinate of a microphone when a one head tom tom drum is excited by the recorded force vector ham1.

```
function a=sim_mem_air_body(n_steps)
% Simulate a tom tom with one drum head
% Needs:
% make_guide.m reflect2d.m reflect3d.m
% blowup.m blowdown.m
% make_membxy.m make_cylinderxy.m
% make_circmask.m

% Initiate parameters of simulation

load hammers.mat

fs=22050                 % Sampling rate
drumsize=0.35            % Diameter of drum
Zair=410                 % Air impedance
Zmemb=0.045              % Membrane impedance
```

43

```
dl=sqrt(2)*53/fs;          % Membrane waveguide length
ds=sqrt(3)*340/fs;         % Air waveguide length
A=dl*dl                    % Area of membrane element

cyldep=round(0.25/ds)      % Depth of drum body in junctions
diam=round(drumsize/dl) % Diameter of membrane junctions
r=round(diam/2)            % Radius of membrane junctions
sx=diam+2;sy=diam+2;       % Size of Membrane waveguide
cx=round(sx/2);            % Center coordinate if membrane
cy=round(sy/2);

% Create Air wave guide mesh (3D)
air=make_guide(3,75,75,75,1/Zair);
fair=zeros(75,75,75);
% Neumann boundary conditions in air
air=make_membxy(air,38-7,38-7,38+7,38+7,38,38,-1e9);
air=make_cylinderxy(air,38-7,38-7,38+7,38+7,38-cyldep,38,-1e9);

mask=make_circmaskxy(12,12,1,1,12,12);
mask2=blowup(mask,105/12);

% Create membrane wave guide mesh (2D)
e=make_guide(2,sx,sx,1,Zmemb);
f=zeros(sx,sx);
% Dirichlet boundary conditions of membrane
e=make_cylinderxy(e,cx-r,cy-r,cx+r,cy+r,1,1,1e9);
% Add air loading
maskmemb=make_circmaskxy(sx,sy,cx-r,cy-r,cx+r,cy+r);
e.ztot=e.ztot+0.5*mask2*2*A*Zair.*maskmemb;

a.snd=zeros(n_steps,1);       % Init recording vector

for t=1:n_steps
    % Convert between membrane and air
    pa=air.vi(38-5:38+6,38-5:38+6,38);
    pb=air.vo(38-5:38+6,38-5:38+6,38);
    f=blowup(2*A*(pb-pa),105/12).*mask2;
    % Insert excitation
    if(t<512)
        f(cx,cy)=f(cx,cy)+ham1(t);
    end
    % Make reflection
    e=reflect2d(e,-f);
    air=reflect3d(air,fair);
    % Draw membrane into airmesh
    v=blowdown(e.v.*mask2,12/105)*((12/105)^2);
    air.vo(38-5:38+6,38-5:38+6,39)=air.vo(38-5:38+6,38-5:38+6,39)+
        Zair*v.*mask;
```

```matlab
air.vi(38-5:38+6,38-5:38+6,37)=air.vi(38-5:38+6,38-5:38+6,37)-
    Zair*v.*mask;
% Record
a.snd(t)=air.v(12,38,64);
end
```

Appendix C   Recording the sound of tom tom drums.

C.1   Introduction

To obtain sound samples of a real drum under documented conditions these experiments were set up and carried out in the anechoic chamber at Chalmers University of Technology. The goal was to get dry sound samples of a tom tom drum being hit at well defined positions with different velocities and exciters. The samples can then be directly related to physical units such as sound pressure of the produced sound wave or impact velocity of the exciter. Two similar series of experiments were carried out on two different tom tom drums.

C.2   Experimental setup

C.2.1   Apparatus used in the experiment

Recording Sound was recorded using a Brüel & Kjær microphone via a preamplifier to a Tascam DAT recorder with 16 bit resolution. The recording level was calibrated using a 94 dB audio test tone at 1000 Hz. The test tone reached the amplitude 18380 of 32767 on the recording.

The signal from the Brüel & Kjær force transducer recorded to DAT via a dedicated preamplifier. The transducer delivered 3.4 pC/N. The amplifier was set to a sensitivity of 10 mV/pC and integration mode in which the signal is attenuated to 1% of the original. The recording level was detected using a 3.9 mV root mean square sine tone at 1000Hz. The test tone reached an amplitude of 4920 of 32767 for the 14″ drum and 5200 for the 15″ drum.

Drums   Two drums were used:
(a) A 14″ (35.6 cm) tom tom made of clear plexi glass with an effective diameter of 35 cm and a depth of 25 cm. The drum heads were held with 6 tuning bolts.

14″ Tom tom	
Effective diameter	0.35 m
Depth	0.25 m
Tuning bolts	6
Material	Plexi glass

(b) A 15″ (38.1 cm) tom tom (Yamaha TT9156A) made of maple in 6-layer plywood with an effective diameter of 37.5 cm and a depth of 30 cm. The drum head were held with 8 tuning bolts.

15″ Tom tom	
Effective diameter	0.375 m
Depth	0.30 m
Tuning-bolts	8
Material	6 ply maple plywood

On both drums two types of Remo Weather-king drum skins were used for the battering head; a simple, one layer head ("clear" on (a) and "smooth white" on (b)) and a two layer head with a thin oil in between ("coated"). The resonant head of (a) was a dedicated resonance head while in (b) a smooth white battering head was used.

Exciters   Three exciters were used in the experiment:

A force transducer mounted on a shaft and used as a hammer (see recording above).

A drum stick made of American maple, weight 80 g.

A drum stick whose tip was clad in felt (3 cm in diameter) to emulate the characteristics of the soft tip on felt mallets used on concert toms.

C.2.2   Placement of drums and microphones

The experiments were conducted in an anechoic chamber with a volume of 800 m^3. The floor of the chamber is made of a net mounted in the middle plane of the room. In the middle of the room there is a staging made out of thin metal that allows stands to be mounted. These were utilized to position the drum and the microphone.

The microphone was mounted on a stand 0.7 m from the platform on which the drum was centered. It had an angle of approximately $45°$ to the battering head of the drum (see fig C.2).

(a)   The drum was mounted on a stand approximately 1m high and the base of the stand was covered with glass fiber wool to minimize reflections from the platform it was placed on.

(b)   The drum mounting mechanism of this drum proved to be incompatible with the round bar used to attach the first drum so the drum was hung from the roof in two steel wires extended with plastic string tied in a loop around pairs of opposite tuning bolts. The approximate total length of the
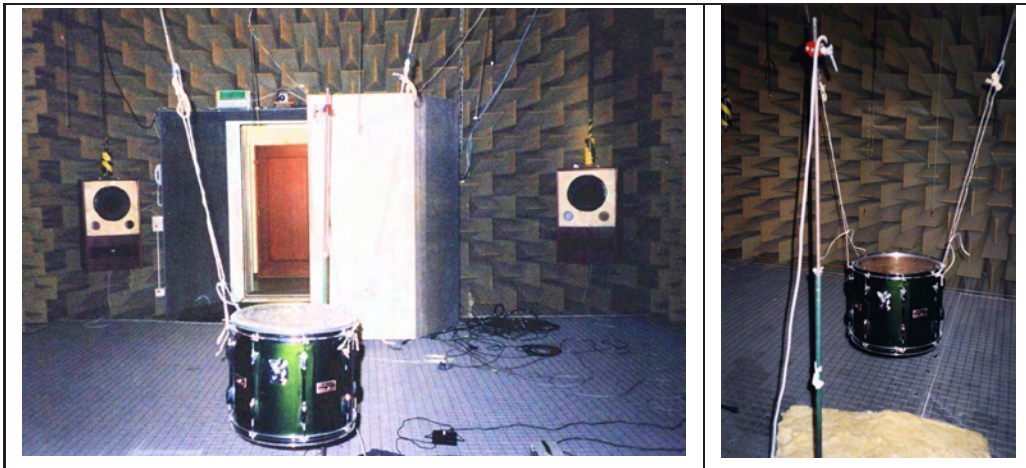
Figure C.1: Photos from the experiment.

extended wires was about 5 meters. Glass fiber wool was used to minimize reflections from the platform below the drum.

The distance between the center of the drum and the stand was 0.74 m in experiment (a) and 0.69 m in experiment (b). The distance between the microphone and the center of the drum remained the same; 0.95 m.

C.3   List of measurements.

The following recordings were made on the two drums:

C.3.1   The 14″ drum (a).

Coated battering head with resonant head.

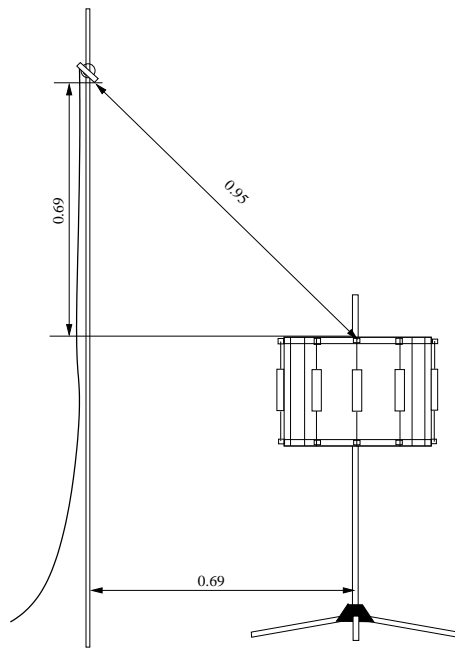| Exciter	Positions
Drum stick	1-3
Felt stick	1-7
Transducer	1-7
Transducer (damped res. head)	1-7
Drum stick (damped res. head)	1
Drum stick (damped bat.head)	1

Coated battering head without resonant head.

Figure C.2: Principal setup of the drum and microphone (distances in meters).

Exciter	Positions
Drum stick	1-7
Transducer	1-7

Clear battering head with resonant head.

Exciter	Positions
Drum stick	1-7
Felt stick	1-7
Transducer	1-7
Transducer (damped res. head)	1-7
Drum stick (damped res. head)	1
Drum stick (damped bat.head)	1

Clear battering head without resonant head.

Exciter	Positions
Drum stick	1-7
Transducer	1-7

C.3.2 The 15″ drum (b).

Coated battering head with resonant head.

Exciter	Positions
Drum stick	1-3
Felt stick	1-7
Transducer	1-7
Transducer (damped res. head)	1-7
Drum stick (damped res. head)	1
Drum stick (damped bat.head)	1

Coated battering head without resonant head.

Exciter	Positions
Drum stick	1-7
Transducer	1-7

Smooth white battering head with resonant head.

Exciter	Positions
Drum stick	1-7
Felt stick	1-7
Transducer	1-7
Transducer (damped res. head)	1-7
Drum stick (damped res. head)	1
Drum stick (damped bat.head)	1

Smooth white battering head without resonant head.

Exciter	Positions
Drum stick	1-7
Transducer	1-7

Care was taken to ensure that hits without multiple excitations of the head were recorded striking at three subjective levels, soft, medium and hard. Each excitation was given time to die out before moving on to the next. Samples were taken hitting the battering and resonant head with the other membrane damped with a soft cloth to get the characteristics resonant frequencies of the individual heads as well.
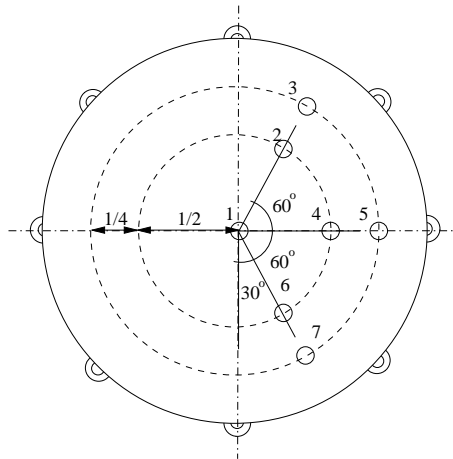
Figure C.3: Positions of the selected excitation areas
the microphone is placed in the direction of $0°$.

C.4 Analysis

C.4.1 Analysing the overtones at different excitation points

The diagrams in figure C.4 to C.7 consist of the peaks of the frequency spectrum of the drum sample. The frequencies are calculated from the first 0.5 s of the sample. The decay times are then calculated as the time it takes the signal to reach an amplitude of 0.001 of the initial amplitude (i e -60 dB).

Considering the first resonant frequencies it is possible to see that exciting the head in points 2 and 3 excites the second and third resonances more than when excited in point 1. This is because these frequencies correspond to the zeroes ξ_{11} and ξ_{21} of the Bessel function which are both unaxisymmetric with an angular dependence and therefore must be excited by an unaxisymmetric hit.

Decay times seem to be unaffected by the point of excitation relative to each other. This is expected as the excitation in the ideal case should only affect the initial amplitude.

The difference between The single layer head (fig C.4, C.5) and the double layer head (fig C.6, C.7) seems to be a shift of the long decay times towards lower frequencies which can be heard in the samples as a darker decay sound of the double layer head.

C.4.2 Examining the effects of air loading.

Air loading is expected to do the following compared to the ideal membrane (according to [4], chapter 3):

- The resonant frequencies are lowered. The fundamental is lowered the most.

- Resonances connected to nonaxisymmetric solutions are lowered more.
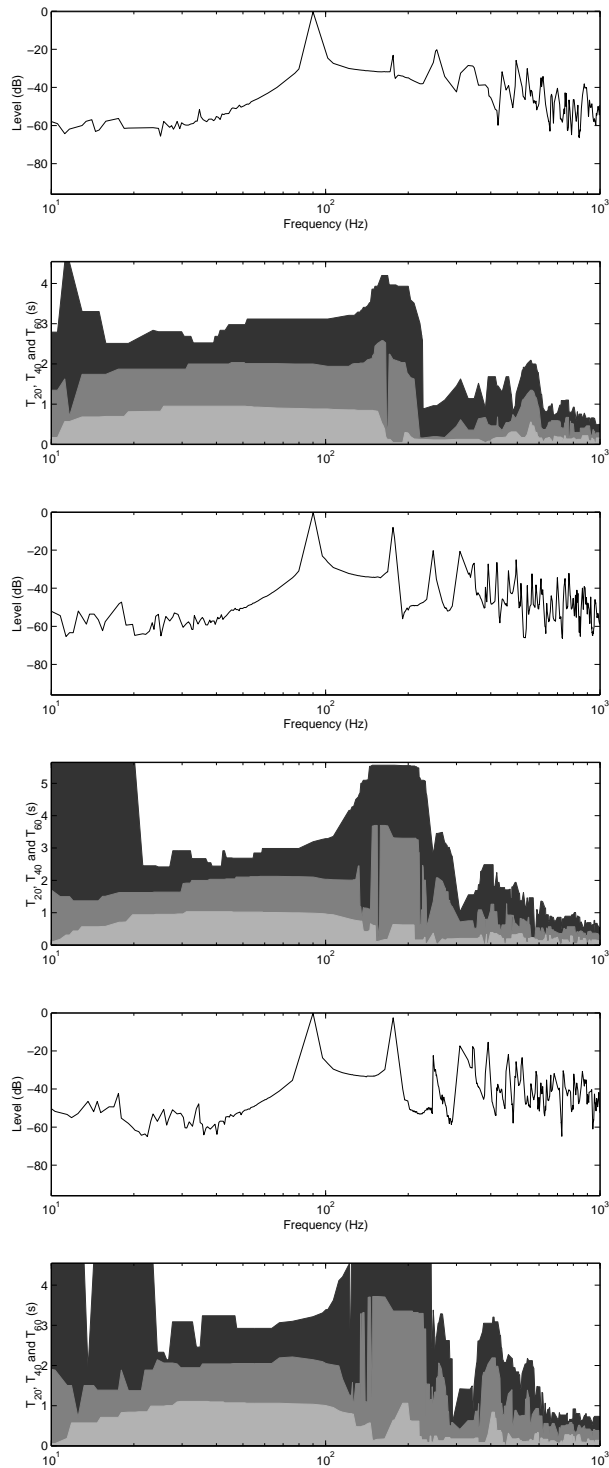
Figure C.4: The amplitudes and decay times of drum (a) with a single layer battering head, without resonant head, hit with a drum stick at positions 1, 2 and 3.
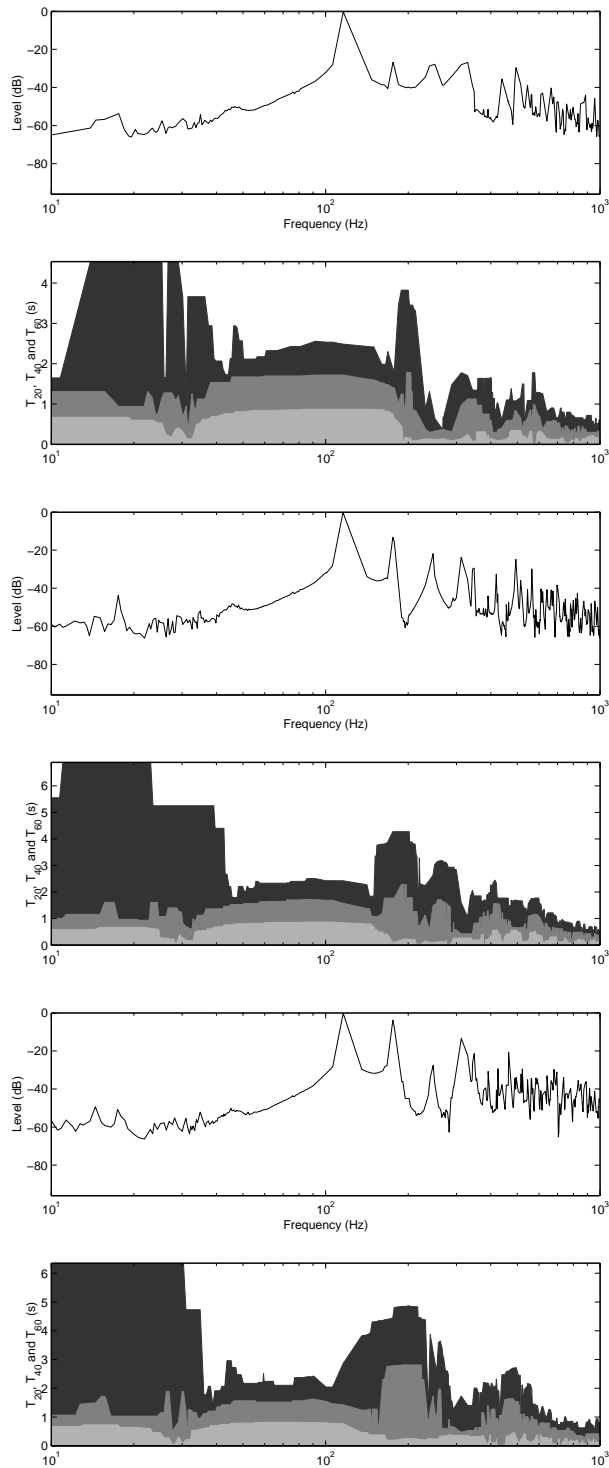
Figure C.5: The amplitudes and decay times of drum (a) with a single layer battering head, with resonant head, hit with a drum stick at positions 1, 2 and 3.
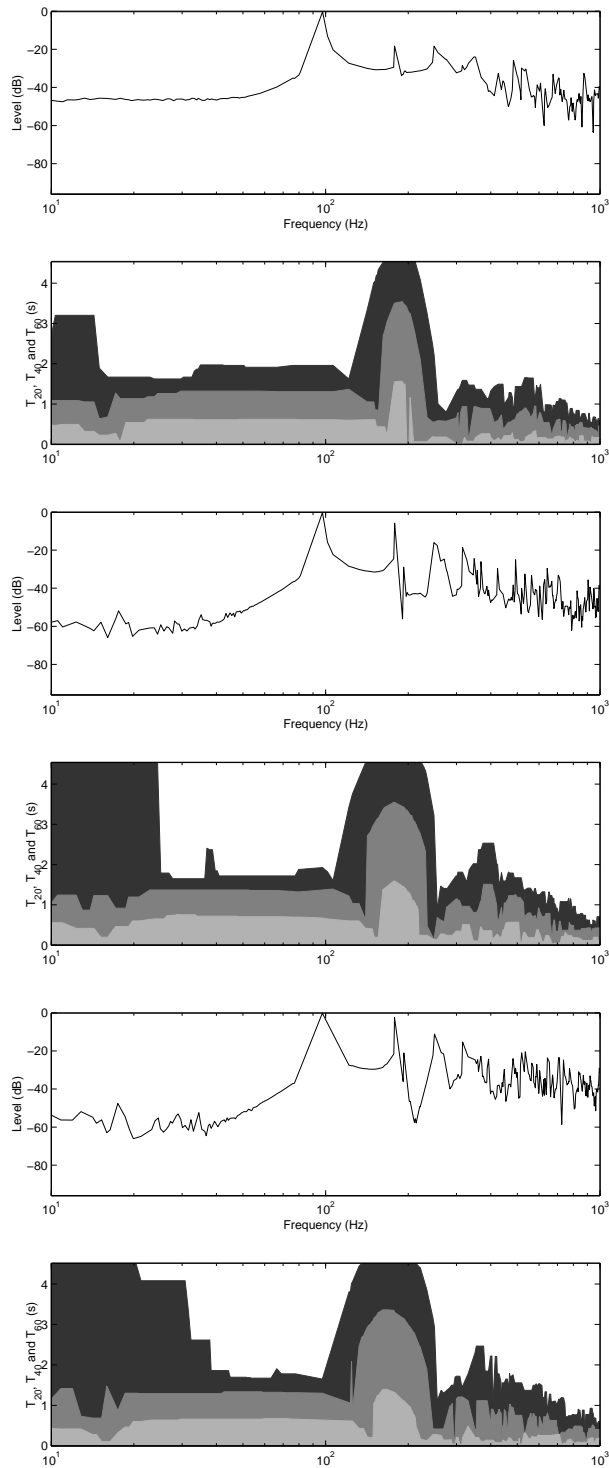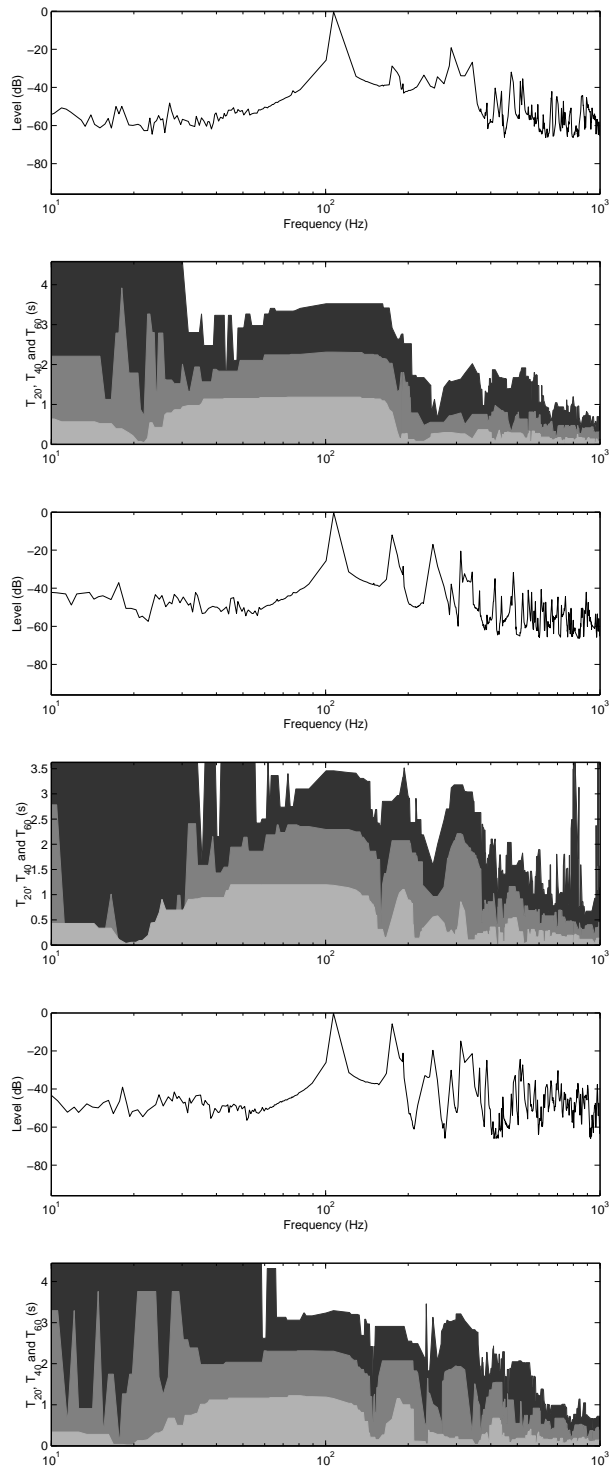
Figure C.6: The amplitudes and decay times of drum (a) with double layer battering head, without resonant head, hit with a drum stick at positions 1, 2 and 3.

Figure C.7: The amplitudes and decay times of drum (a) with a double layer battering head, with resonant head, hit with a drum stick at positions 1, 2 and 3.

- Enclosed air favours the resonances of axisymmetric solutions .

As low frequencies are affected the most by the airloading a good assumption is to assume that a higher resonance corresponds better with the resonances of the ideal membrane. Therefore ξ_{02}, which is the fourth resonance, is chosen to connect the resonances of the drum samples to the corresponding ideal membrane. Higher resonances are more difficult to pin point.

ξ_{01}/ξ_{02}	ξ_{11}/ξ_{02}	ξ_{21}/ξ_{02}	ξ_{02}/ξ_{02}	ξ_{31}/ξ_{02}
0.4356	0.6941	0.9303	1	1.156

The first resonant mode of the air enclosed in the body of drum (a) without a resonant head should be $f = \frac{c}{4d} = \frac{340m/s}{4\cdot0.25m} = 340Hz$ where c is the propagational speed of sound in air and d is the depth of the drum. For drum (a) with resonant head this resonance should occur at $f = \frac{c}{2d} = \frac{340m/s}{2\cdot0.25m} = 680Hz$. On drum (b) this should be 283 Hz without and 567 Hz with the resonant head. Around these frequencies there should be a general increase of decay times in the samples (as can be seen in figure C.4 and forward). These have been marked by a shorter line in figure C.8 and C.9. The relation between the fundamental frequency, the speed of propagation, c, and the diameter of the ideal membrane is $f_{01} = \frac{2.4048c}{\pi d}$. The unloaded velocities calculated in table C.1 and C.2 are based on this formula and should be an indication of what the speed of propagation would be of an unloaded drum head. In the measurements of the two head drums with one head damped the lower frequencies were unfortunately so damped that they could not be detected properly. If this is a fundamental observation or a result of the measuring is not evident.

Table C.1: Properties of drum (a) with a single layer battering head ($f_{02} \approx 260Hz$). Resonant head; $f_{02} \approx 373Hz$.

Heads of the drum	Unloaded velocity (m/s)	Unloaded f_{01} (Hz)	Loaded f_{01} (Hz)	Loaded f_{11} (Hz)
Only a battering head	53	113	90.3	177
Damped resonant head	53	113	(78,103)	174
Damped battering head	75	162	(77,103)	248
Battering + resonant head	-	-	116	176

C.4.3 Examining the initial membrane tensioning.

When the battering head is excited the tensioning changes the properties of the membrane. The tension causes an initial upward change of the resonant frequencies. To

Table C.2: Properties of drum (b) with a single layer battering head ($f_{02} \approx 300Hz$).
Resonant head; $f_{02} \approx 386Hz$.

| Heads of the drum	Unloaded velocity (m/s)	Unloaded f_{01} (Hz)	Loaded f_{01} (Hz)	Loaded f_{11} (Hz)
Only a battering head	65	130	94	193
Damped resonant head	65	130	?	199
Damped battering head	84	168	?	243
Battering + resonant head	-	-	129	201
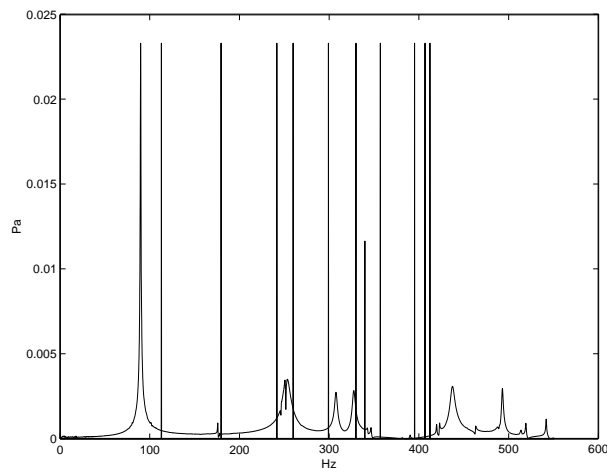
Figure C.8: Spectrum of drum (a) struck at position 1 with a single layer battering head and no resonant head, the resonance frequencies of an ideal membrane adjusted to ξ_{02} are marked with lines.
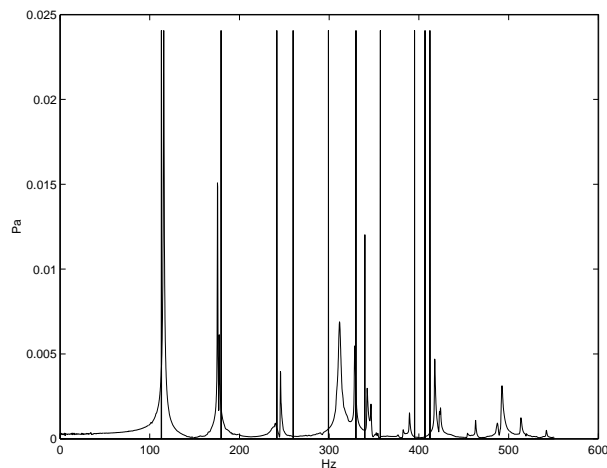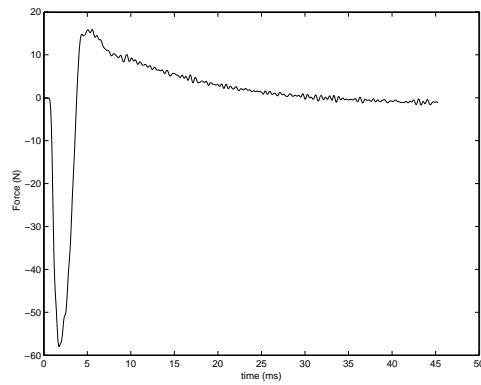

Figure C.9: Spectrum of drum (a) struck at position 1 with a single layer battering head and a resonant head, the resonance frequencies of an ideal membrane adjusted to ξ_{02} are marked with lines.
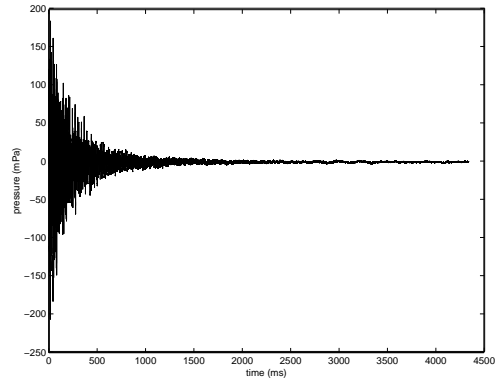
(a) The entire recorded sound.
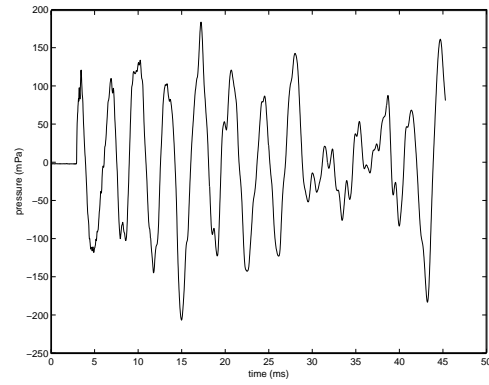
(b) The 50 first milliseconds of the sound.

(c) The force applied to the transducer while hitting the drum head.

Figure C.10: The result of the 14″ drum hit in position 5 with the force transducer hammer.

examine this phenomenon the sound samples were lowpass filtered to isolate the fundamental frequency. Then the inital frequency was compared to the final frequency and the percentual pitch shift was calculated. Samples from the force transducer hitting the 14″ drum with a single layer head and no resonant head were used to be able to relate the shift to the peak force applied to the membrane. The signal was filtered using a Chebyshev type I IIR 6 pole lowpass filter with a cutoff frequency of 110 Hz and a passband ripple of 10 dB. The results are presented in table C.3. The force measured by the transducer is presented within parenthesis in the table. In comparison to the relatively light hammer a hard strike with a drum stick at position 1 produces a pitch shift of almost 8%.

Table C.3: Percentual pitch shift of the fundamental frequency.

Striking strength \ Position	1	2	3
Soft (Force (N))	0(8)	0(15)	-
Medium	-	-	1(20)
Hard	3(36)	3(32)	3(35)

C.4.4 Comparing the felt mallet to the drum stick

The sound of the tom tom struck by a felt mallet is perceptually softer than the sound produced by a drum stick. Figure C.11 contains the resonances and their decay times for the same drum excited in position 1 with (a) a felt mallet and (b) a drum stick. Above 500 Hz the amplitudes of the drum excited by the felt mallet are significantly lower than the amplitudes of the drum excited by a stick (relative to the drums fundamental).

C.4.5 Analysing the force exerted on the head by the force transducer.

The force transducing hammer used in this experiment was very light and gave a sound closer to that of hitting a drum with a heavy pencil than a drum stick. However, the similarities are probably enough to describe the interaction between a drum stick and the drum head. The hammer samples have been differentiated to restore the data to force and then filtered with a 8 pole Chebychev II IIR lowpass filter with a cutoff frequency of 440 Hz (attenuation 40 dB) to lower the noise floor. As can be seen in figure C.12 to C.14 the time of the interaction is approximately constant (around 4-5 ms), roughly corresponding to the time it takes the a moving wave to rebound and then start to throw the drumstick back from the membrane. The shape of the force curve seems to be similar for different striking forces and positions with a slightly sharper peak for higher striking force.
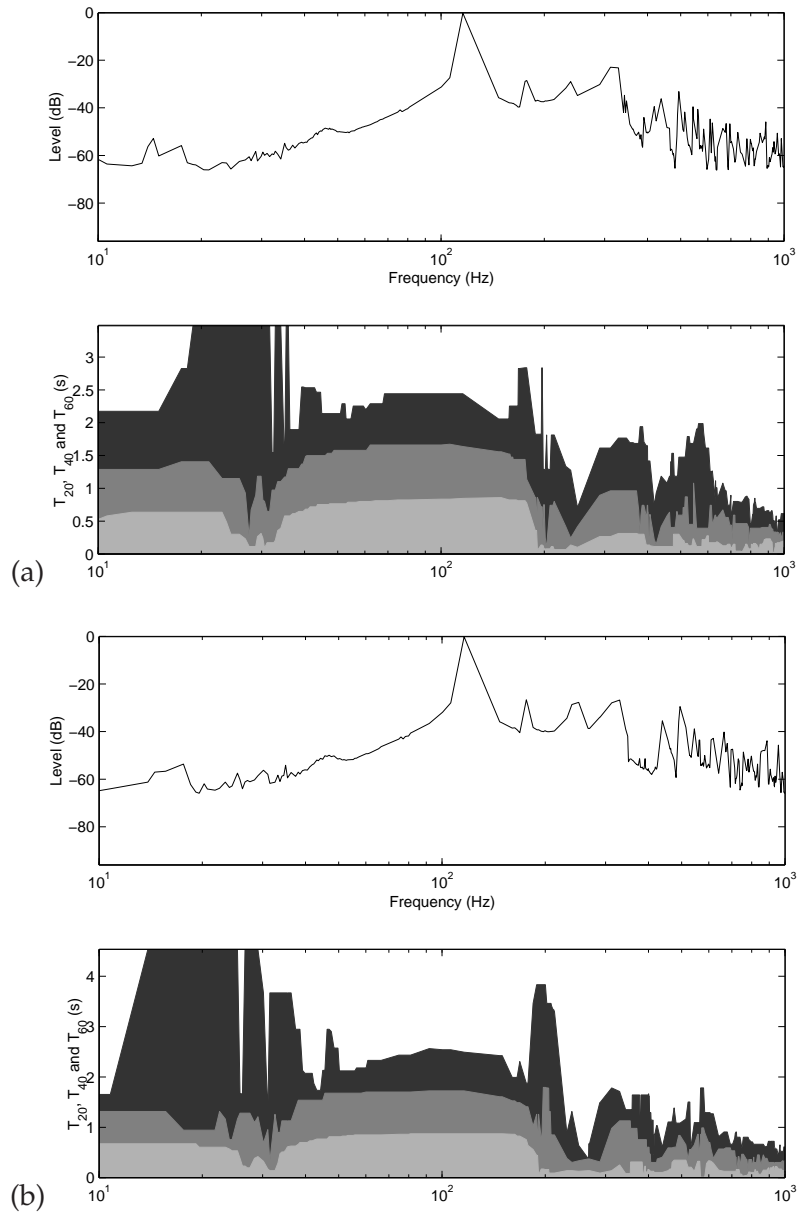
Figure C.11: The amplitudes and decay times of a drum hit by (a) a felt mallet and (b) a drum stick overtones.
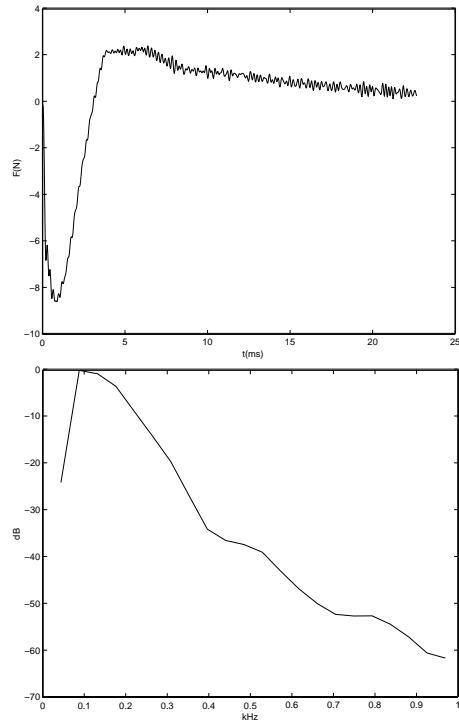
Figure C.12: The force between the head and hammer caused by a soft hit at position 1 to drum (a).

C.5 Conclusion

These recordings reveal many properties of the tom tom drum that can be used as base for modeling drums and evaluating the results.
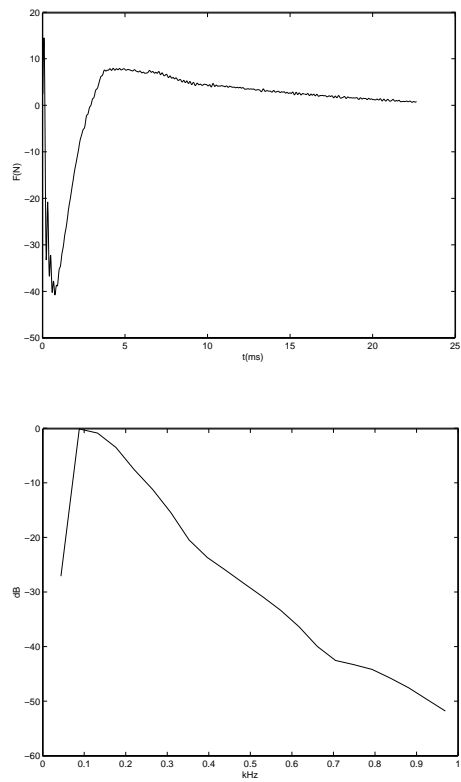
Figure C.13: The force between the head and hammer caused by a hard hit at position 1 to drum (a).
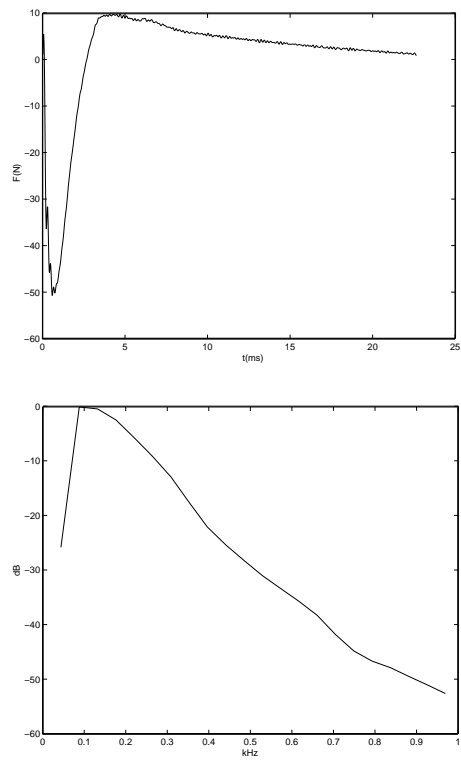
Figure C.14: The force between the head and hammer caused by a hard hit at position 1 to drum (b).

Bibliography

[1] C. Christopoulus. *The Transmission-Line Modeling Method TLM*, ISBN 0-7803-1017-9 IEEE Press (1995).

[2] K. Karplus and Alex Strong. *Digital Synthesis of Plucked-String and Drum Timbres*, Computer Music Journal, Vol. 7, No. 2, pp 43-55, (1983).

[3] D. Jaffe and J.O. Smith. *Extensions of the Karplus-Strong Plucked String Algorithm*, Computer Music Journal, Vol. 7,No. 2, 1983, pp 56-69, (1983).

[4] N.H. Fletcher and T.D Rossing. *The Physics of Musical instruments, second edition*, ISBN 0-387-98374-0 Springer-Verlag (1998).

[5] T. Kihlman. *Grundläggande teknisk akustik, andra upplagan*, Applied Acoustics, Chalmers University of Technology (1983).

[6] S.A. Van Duyne and J.O. Smith. *Physical Modeling with the 2-D Digital Waveguide Mesh*, ICMC Proceedings, Tokyo (1993).

[7] F. Fontana and D. Rocchesso. *Physical Modeling of Membranes for Percussion Instruments*, ACUSTICA Vol. 84 529-542 (1998).

[8] L. Savioja and V. Välimäki. *Reduction of the dispersion error in the interpolated digital waveguide mesh using frequency warping*, http://www.acoustics.hut.fi (1999).

[9] L. Savioja and V. Välimäki. *Improved discrete-time modeling of multi-dimensional wave propagation using the interpolated digital waveguide mesh*, ICASSP'97 vol. 1 pp 459-462, Munich, 1997.

[10] L. Savioja. *Improving the three-dimensional digital waveguide mesh by interpolation*, NAM 98 pp. 265-268, Stockholm (1998).

[11] T.I. Laakso, V. Välimäki, M. Karjalainen and U.K. Laine. *Splitting the Unit Delay*, IEEE Signal Processing Magazine January 1996 pp. 30-54 (1996).

[12] M. Kahrs, K Brandenburg et al. *Applications of digital signal processing to audio and acoustics*, ISBN 0-792-38130-0 Kluwer Academic Publishers (1998).

[13] S.A. van Duyne, J.R. Pierce, J.O. Smith. *Traveling Wave implementation of A lossless Mode-Coupling Filter and The Wave Digital Hammer*, ICMC Proceedings (1994).

[14] A. Fettweis. *Wave digital filters; theory and practice*. Proceedings IEEE74 (1986).

[15] M.-L. Aird. *Musical Instrument Modelling Using Digital Waveguides*, Ph. D. thesis, University of Bath (2002).

[16] J. Laird. *The physical modelling of drums using waveguides*, Ph. D. thesis, University of Bristol (2001).

[17] J. Dattorro. *Effect Design Part 2: Delay-Line Modulation and Chorus*, J. Audio Eng. Soc. vol 45 No 10 (1997).

[18] S. Bilbao. *Wave and Scattering Methods for Numerical Simulation* , ISBN 0-470-87017-6 Wiley (2004)